Rijksuniversiteit Groningen

Bachelor's Thesis

GUSTO: Testing Early Milky Way ISM Data in The [NII] Band

Author:
B.J Moltzer
S5211247

Supervisor:
dr. R.F Shipman

Abstract

Early data from the GUSTO space mission in the [NII] band will be tested by looking at sequences 50 and 51. This will be achieved by calibrating these sequences and forming spectra for the observations of Eta Carinae 5 from mixers 2 and 3. Within these spectra, the [NII] emission at 1.46 THz will be searched for. Moreover, the positions of the scans within these sequences will be extracted. After performing this analysis, differences between the two sequences are found. Sequence 50 consists of two positions, a source and a reference position, separated by around 20.3 arcminutes, making it a standard Point Switch (PS) observation, while sequence 51 consists of a 9-position 16×16 arcminute grid, containing 8 source positions and 1 source and reference position, making it a non-standard PS observation. The positions given from the sequences are far from the actual region of Eta Carinae 5 due to the star-tracker data being incorrectly coupled during sequences 50 and 51. In both these sequences, for mixers 2 and 3, no [NII] emission features can be found, thus indicating the absence of [NII] emission.

Acknowledgements

I want to thank my first supervisor, Russell Shipman, for his active help and guidance throughout the entire thesis project. Moreover, I would like to thank Silke Oosterhof for her help while working together on the GUSTO data. Finally, I appreciate my friends and family who kept me motivated during the project. Aside from this, I'd like to acknowledge the usage of AI tools like ChatGPT, which I used to provide assistance during code debugging and formatting issues.

Contents

1 Introduction

The interstellar medium (ISM) is the region between stars within a galaxy. By studying this region, the dynamics of a galaxy can be determined. For astronomers, observing and studying the ISM is therefore a must. This can be achieved by looking at the properties of the ISM, allowing astronomers to infer important regional features, like a potential star-forming region (SFR) (Draine, 2011). Spectroscopy is the primary and most effective observational method used to uncover these features, where atomic and molecular transitions into excited or de-excited levels can be detected using their interaction with light (Draine, 2011). In our local galaxy, the most precise and strongest fine-structure lines that can be detected are [Hα] and [Hβ] in the optical regime. On the other hand, fine-structure lines found in the terahertz regime are faint and tough to capture. In the case of these terahertz lines, ground-based observations cannot be used. This is due to the high opacity of the Earth's atmosphere at high wavelengths, which blocks the detection of such lines (Thomas L. Wilson, 2009). Therefore, such lines can only be detected using an observatory outside the Earth's atmosphere. Thus, high altitude observatories containing far-infrared spectroscopic instruments that observed within the stratosphere, like SOFIA (Heyminck, Graf, et al., 2012) and outside, like Herschel (Persson, Gerin, et al., 2014), were able to detect these terahertz lines.

One such observatory is the Galactic/Extragalactic ULDB Spectroscopic Terahertz Observatory (GUSTO) (Fig. 1). Similar to SOFIA, this balloon-based observatory observed the Milky Way's ISM from the Earth's stratosphere (Silva, Laauwen, et al., 2023). The GUSTO project was primarily funded by NASA, which launched it as part of their Explorers Program, specifically as a Mission of Opportunity (Smith, 2025). Its predecessor, the Stratospheric Terahertz Observatory 2 (STO-2), after a successful flight in 2016, managed to prove the viability of balloon-based space missions and the possibility of a larger balloon-based mission (NASA, 2015). With Prof. Chris Walker from the University of Arizona as the principal investigator, working together with NASA's Jet Propulsion Laboratory (JPL), the Massachusetts Institute of Technology (MIT), SRON and APL from John Hopkins University, the technologies and structures required for the GUSTO payload were created, and the mission was coordinated (Smith, 2025). This payload includes the telescope, three sets of heterodyne receiver arrays, autocorrelator spectrometers, instrument control electronics and a cryostat that can cool the instruments to a temperature of 4K. This payload was mounted onto a 0.9-meter-tall gondola (Walker, Kulesa, et al., 2022).

GUSTO was successfully launched on the 31st of December 2023 from Antarctica. GUSTO remained mission active for 57 days, whilst floating at an altitude of around 35-40 km in the stratosphere above the South Pole. During its flight, due to the polar vortex present at the South Pole, GUSTO spiralled out towards the north, allowing it to capture more of the Milky Way (Silva, Laauwen, et al., 2023).

GUSTO surveyed the Large Magellanic Cloud for an area of 2 deg^2. It surveyed the galactic plane at a galactic longitude (b) of $|b| \leq -1.2°$ and a galactic latitude (l) around $2.7° \leq l \leq -28°$ for an area of around 62 deg^2 (Walker, Kulesa, et al., 2022). Its purpose was to probe and study star formation processes and the dynamics of clouds in the interstellar medium (ISM). This includes understanding the lifecycle of gas in the ISM, understanding the dynamics of gas in- and outflow in the galactic centre, understanding the interactions between star formation, stellar winds, radiation and ISM structure and finally forming a template of these understandings for galaxies outside of our local universe (Silva, Laauwen, et al., 2023).

During the mission, GUSTO aimed to detect the THz fine-structure lines of [CII] at 1.9 THz, [NII] at 1.46 THz and [OI] at 4.7 THz. It aimed to capture these lines using a 4×2 hot electron bolometer (HEB) array of mixers (Silva, Laauwen, et al., 2023). Additionally, GUSTO could velocity resolve these lines, meaning that the respective velocities of the gas carrying the atomic transitions could be directly determined.

As previously stated, GUSTO used a heterodyne receiver to detect the THz fine-structure lines. A heterodyne receiver system is a receiver technology that captures electromagnetic radiation and downconverts it to a lower intermediate frequency (IF), converting a THz frequency signal to a GHz frequency signal in the radio regime. This IF can then be amplified and analysed at a high sensitivity (Thomas L. Wilson, 2009). The success of this type of receiver in observatories like ALMA, Herschel, and SOFIA has led to significant advancements in terms of precision and sensitivity for heterodyne receivers. (Silva, Laauwen, et al., 2023).

This project uses data from the initial stages of the post-launch phase of GUSTO. During this phase, GUSTO was operated with the primary aim of determining and calibrating its pointing. Therefore, scans of well-known interstellar medium (ISM) regions, like the Carinae region, were taken. Since during this early phase of the mission, GUSTO was not focused on performing clear scans of the galactic plane or the LMC, the data from this initial phase contains many inconsistencies, as will become clear during this thesis.

This thesis aims to test the GUSTO heterodyne receiver system, its data products, and the observing procedures by analysing potential [NII] observations during the initial post-launch stages of the high-altitude observatory. This thesis will have a structure where in Sect. 2, the methods and theory of the observational principles and the Milky

Way ISM will be discussed. In Sect. 3, the observational properties of GUSTO and the data reduction will be presented. In Sect. 4, the project's results will be showcased. In Sect. 5, the found results will be discussed, including supposed [NII] emission features. Finally, Sect. 6 will outline the conclusions of this thesis and potential improvements.

Figure 1: Image showing the Galactic/Extragalactic ULDB Spectroscopic Terahertz Observatory (GUSTO) prior to its launch in Antarctica (SRON, 2025).

2 Method and Theory

2.1 GUSTO Cataloging

An important point of clarification when handling the GUSTO data is knowing what a sequence is. As defined later during the mission by the GUSTO team, a sequence is a group of individual scans that, when bundled together, form a calibratable group of data that can be used to create a spectrum.

These sequences additionally have certain observation types. These observation types help define the observational goal of the sequence. One of these types is a Position Switch (PS) observation. Here, scans are taken at an on and off-source position for an equal amount of time. This observation type was used during the early stages of the GUSTO mission. Later during the mission, when observing the galactic plane and the LMC, GUSTO switched to On-The-Fly (OTF) observations. In this observation type, scans are taken whilst moving between two points on the sky. This OTF observation was used at a constant longitude along the plane when mapping the galactic plane.

Additionally, the scans in a sequence consist of 4 types of measurements. These include a source measurement, a source-hot measurement, a reference measurement and a reference-hot measurement. These subtypes of scans are crucial for data calibration, as will later be explained in Sect. 3.2.

2.2 Heterodyne Receivers

Heterodyne receivers are commonly used in telescopes to measure high-frequency lines. Most notably, heterodyne receivers were included in the SOFIA and the Herschel space missions, yet they are also used on the ground in observatories like the Atacama Large Millimetre Array (ALMA). As stated in Sect. 1, a heterodyne receiver system's purpose is to downconvert the electromagnetic radiation's captured frequency to a lower intermediate frequency. A heterodyne receiver system has multiple components that help achieve this goal (Fig. 2). Firstly, the captured radiation is mixed in the mixer with the strong signal produced by the local oscillator. After this mixing, an absolute difference is taken between the two frequencies, resulting in the IF, given by the formula:

$$f_{IF} = |f - f_{LO}| \,. \tag{1}$$

Here, f is the signal frequency and f_{LO} is the local oscillator frequency. The resulting frequency f_{IF} can have two elements. The first element occurs when $f > f_{LO}$, resulting in an upper sideband (USB) and the second element occurs when $f < f_{LO}$, resulting in a lower sideband (LSB). These two elements can then either be added together, which occurs in a double sideband (DSB) mixer, or they can be given separately, which appears in a single sideband (SBB) mixer (Silva, Laauwen, et al., 2023).

When downconverting to the IF, a relatively weak signal is produced. Thus, the IF must be amplified by an amplifier to strengthen the signal and to achieve a better gain (Lin & Jarrahi, 2020). The resulting signal is then filtered for unwanted frequencies and excessive noise (Lin & Jarrahi, 2020). Finally, after this filtering process, a clean signal is produced that can be analysed by the spectrometer. To better understand the inner workings and types of parts in a heterodyne receiver, the following sub-chapters will elaborate upon this. Then, in Sect. 3.1, the specific types of parts used within GUSTO's heterodyne receiver will be given.

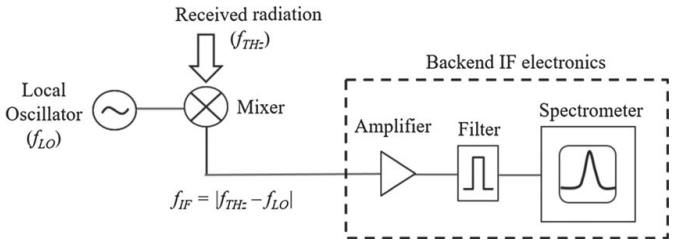

Figure 2: Figure showing the basic principles of a heterodyne receiver system in terahertz spectroscopy. This includes the local oscillator, the mixer, the amplifier, the filter and finally the spectrometer. (Lin & Jarrahi, 2020)

2.2.1 Mixers

Within a heterodyne receiver system, the mixer has the important role of forming the downconverted IF from the initial high-frequency signal. In the case of terahertz astronomy, the most commonly used types of mixers are Schottky diode mixers and superconductive hot electron bolometer (HEB) mixers (Silva, Laauwen, et al., 2023).

The Schottky diode mixer is a mixer that uses Schottky diodes, a type of metal semiconductor diode (Physical Research Laboratory, 2007). The main advantage of a Schottky diode mixer is that it can operate at room temperature. Thus, it does not need to be cryogenically cooled, making it easy to implement within a heterodyne receiver. Moreover, the mixer has a high frequency range of 0.1-4.7 THz (Mehdi, Siles, et al., 2017), thus allowing it to capture high frequency lines. On the other hand, a Schottky diode mixer has a relatively low sensitivity compared to different mixer types (Silva, Laauwen, et al., 2023). Thus, this mixer is often outperformed, yet it is easy to implement because it is not dependent on cryogenics.

Besides this, hot electron bolometer (HEB) mixers use the bolometric effect in a superconducting material (W. Zhang, Miao, et al., 2022). Here, due to the incoming radiation being absorbed, there is an increase in temperature, further increasing electrical resistance and thus a measurable effect (W. Zhang, Miao, et al., 2022). In a HEB, this effect occurs at temperatures around 0K, where electrons are heated due to captured radiation above the temperature of phonons in the diode (Richards, 1994). To reach those temperatures, this type of mixer must again be cryogenically cooled. This mixer can operate between frequencies of 0.3-6 THz and has a high sensitivity (Silva, Laauwen, et al., 2023). Due to this frequency range having a high upper limit, weak THz fine-structure lines can now be detected. This type of mixer is used in instruments like Herschel's HIFI (de Graauw, Helmich, et al., 2010) and SOFIA's upGREAT (Heyminck, Graf, et al., 2012) to help detect THz fine-structure lines.

2.2.2 Local Oscillator

To successfully form an IF, a local oscillator (LO) must be present, generating a strong and constant signal for the down-conversion to the IF. Therefore, optimal LO sources must be present to achieve high-frequency stability. In terahertz astronomy, these sources mainly include Far Infra-Red (FIR) Gas lasers with a Schottky diode-based frequency multiplier chains or, most recently, a quantum cascade laser (QCL) (Silva, Laauwen, et al., 2023).

FIR Gas lasers are frequency tunable lasers of excited gas (Richter, Greiner-Bär, et al., 2010). In the case of SOFIA's GREAT instrument, this gas consisted of radio frequency excited CO_2, of which the frequency was tunable using a grating (Richter, Greiner-Bär, et al., 2010). The power of this laser can then be amplified by using a frequency multiplier chain. This type of laser provides a general high amount of power, can operate at terahertz-level frequencies less than 2 THz and can operate at room temperatures, thus not requiring cooling (Silva, Laauwen, et al., 2023). The main issue with this LO source is that the power decreases significantly at higher frequencies (Silva, Laauwen, et al., 2023), which is not optimal for a terahertz observatory LO that requires a strong signal.

A QCL is a semi/super-conductor material-based laser (Betz, Boreiko, et al., 2006). Consisting of multiple quantum wells from alternating low and high-bandgap materials, a QCL can emit photons as electrons that transition between the quantum wells (Betz, Boreiko, et al., 2006). By changing the quantum wells' size, the beam's frequency becomes interchangeable (Betz, Boreiko, et al., 2006). Thus, this produces an interchangeable frequency-stable beam, perfect for a modern local oscillator. Moreover, the power of a QCL is frequency-dependent. A higher frequency produces a high QCL power (Silva, Laauwen, et al., 2023). Therefore, when looking at THz lines like [NII] at 1.46 THz, a QCL becomes a viable option.

2.3 The Interstellar Medium

The Interstellar Medium (ISM) is the astrophysical region between stars that contains matter, in the form of dust and gas, and radiation. The ISM is dynamic; therefore, due to the movement of particles it contains, hydro-physical phenomena like turbulence are given rise to.

The most abundant atom within the ISM is hydrogen. Hydrogen in the ISM can be either neutral (HI), ionised (HII) or molecular (H_2). Within the Milky Way, 60% of hydrogen is HI, 23% is HII, and 17% is H_2 (Draine, 2011). Characteristic phases can represent the dust and gas in the ISM. The most common form is warm ($T \sim 5000\ K$) and hot ($T \sim 10^{5.5}\ K$) ionised gas, called the Warm ionised Medium (WIM) and the Hot ionised Medium (HIM) or Coronal Gas (Draine, 2011). Moreover, there are ionised hydrogen (HII) regions ($T \sim 10^4\ K$) within the ISM that are formed due to the photoionisation of gas by hot stars (Draine, 2011). These regions are commonly found in regions called OB-associations. These associations contain very hot O- and B-type stars, which are a source of a lot of radiation that can thus photoionise the surrounding gas and maintain photoionisation (Draine, 2011). Aside from this, the ISM contains dense ($n_H = 10^3 - 10^6\ cm^{-3}$) and diffuse ($n_H = 10^2\ cm^{-3}$) molecular gas ($T \sim 10 - 50\ K$) (Draine, 2011). These regions are H_2 self-shielded, allowing them to protect themselves from photo-disassociation, meaning that the molecules at the centre of a molecular gas cloud cannot be broken down by photons (Draine, 2011). The dense molecular clouds are often CO-dark, meaning that the surface's carbon monoxide (CO) molecules are UV photo-dissociated. Whilst being CO-dark, these clouds can still be detected due to photo-dissociation breaking down the molecule into C and O. These atoms can then be excited, forming fine-structure lines that are detectable, like [CII] and [OI]. These clouds are important when trying to understand stellar evolution since, within these dense clouds, star formation takes place (Draine, 2011). All these regions and phases help define the ISM and its atomic and molecular constituents.

2.4 [NII] Emission

In the context of the ISM, [NII] is a tracer of ionised gas. This makes [NII] an important tracer when aiming to observe stellar evolution, since this ionised gas is present during the initial phases of star formation (Draine, 2011). Moreover, nitrogen is an abundant element in the ISM, making it an ideal tracer.

Nitrogen has two relevant emission features in the terahertz regime (Tab. 1). Compared to other nitrogen fine-structure lines, these THz features are relatively weak and are more difficult to detect. This is because these fine-structure lines occur due to the magnetic dipole transition of nitrogen. This means that emission occurs due to de-excitation from an interaction with the magnetic component of the photon's electromagnetic radiation. On the other hand, this transition is forbidden in the case of the electric dipole moment (Griffiths & Schroeter, 2024), making the transition partially forbidden. Thus, due to these terahertz fine-structure lines being partially forbidden, it is rarer to detect them.

Species → Line	Transition	Frequency (THz)	Excitation Energy (K)
$N^+ \rightarrow$ [NII]	$^3P_2 \rightarrow {}^3P_1$	2.45	188
	$^3P_1 \rightarrow {}^3P_0$	1.46	70

Table 1: Spectroscopic properties of fine-structure lines of singly ionised nitrogen in the terahertz regime. (A. Kramida, Yu. Ralchenko, et al., 2024)

2.5 Eta Carinae

Eta Carinae is a stellar system composed of 2 massive variable stars (Eta Carinae A and B) with a joint apparent magnitude of currently around 4 (Steinmassl, Breuhaus, et al., 2023). It lies at the centre of the Carinae Nebula Complex (CNC) outflow. This complex is around 40 pc in diameter, containing an extended OB association, known as CarOB1 and a bright HII region, known as NGC 3372 (X. Zhang, Lee, et al., 2001). The complex is around 2.35 Kpc away from Earth, with Eta Carinae located at the galactic coordinates: $(l.b) = (287.2°, -0.6°)$ (SIMBAD, 2025). This complex is known for its active star formation, containing many young and old stars. Moreover, photon-dominated regions (PDRs) are generated within the complex due to cloud interactions, generating high flux intensities, like in the north-western regions, where the CNC interacts with the GMC (Kramer, Cubick, et al., 2007). Thus, within this complex, star-formation tracers are bound to be present (Seo, Goldsmith, et al., 2019). Within the Eta Carinae region, bright massive stars like HD 93027 and HD 305536 can be found (SIMBAD, 2025). Due to the strong star-formation conditions present in Eta Carinae, the complex is surrounded by an HII region (X. Zhang, Lee, et al., 2001). Moreover, to sustain star formation, the Carinae complex contains large molecular clouds with a mass of around $10^3 - 10^5\ M_\odot$ (Steinmassl, Breuhaus, et al., 2023). Due to these properties, Eta Carinae is an ideal region for scans for missions like GUSTO that aim to find star-formation tracers like [NII] and [CII].

During the GUSTO mission, two regions were chosen for Eta Carinae, regions 2 and 5, that were classified using the following map (Fig. 3). This map was created by considering the different subcomplexes within Eta Carinae using elements like known OB-associations and cloud-morphology (X. Zhang, Lee, et al., 2001).

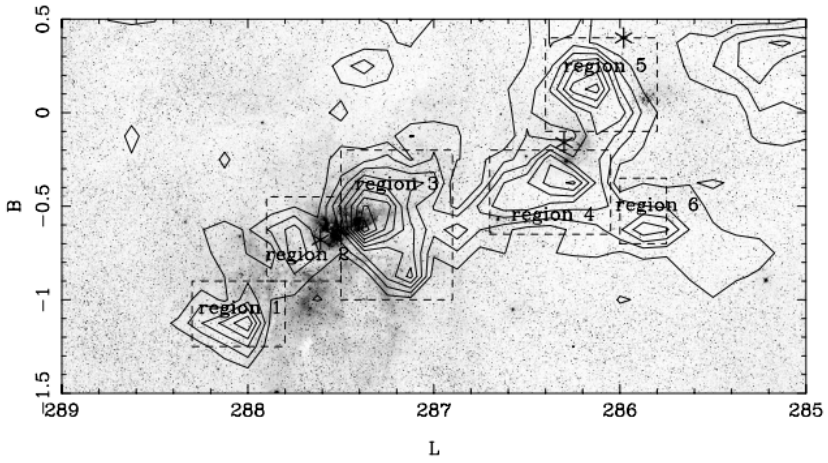

Figure 3: Image displaying the labelling of the 6 regions within Eta Carinae in galactic coordinates as classified by Zhang (X. Zhang, Lee, et al., 2001), where regions 2 and 5 were used during the GUSTO mission.

2.6 Y-factor Calibration

A typical receiver calibration technique used in radio astronomy is the y-factor method. This technique can also be used for heterodyne receivers by downconverting the frequency from THz to GHz. This method uses measurements from a hot and cold load to form a factor that can normalise a spectrum. These loads are calibratable sources with a near-constant temperature, allowing for accurate calibration. By measuring the power response from these loads, the y-factor (Y) is formed (Thomas L. Wilson, 2009):

$$Y = \frac{P_{hot}}{P_{cold,}} \tag{2}$$

where P_{hot} is the measured response of the hot load and P_{cold} is the measured response of the cold source. From this Y-factor, the noise temperature of the receiver T_N can be derived. Assuming a linear response of the system to the incoming signal, the following formula can be applied (Thomas L. Wilson, 2009):

$$T_N = \frac{T_{hot} - T_{sky} \cdot Y}{Y - 1} \tag{3}$$

where T_{hot} is the temperature of a hot load and Y is the Y-factor. To obtain the T_{sky}, the Callen-Welton equation must be applied, which is given to be: (Kerr & Randa, 2010):

$$T_{sky} = \frac{h \cdot f}{2k_b} \tag{4}$$

where h is Planck's constant, f is the frequency and k_b is the Boltzmann constant. Thus, the T_{sky} is linearly frequency dependent. The noise temperature can then be used when generating a spectrum, as will later be described in Sect. 3.2.

2.7 Velocity Resolving

In a heterodyne receiver system, velocity resolution uses the principle of the Doppler shift to estimate a velocity from an intermediate frequency (IF). Therefore, the velocity (v) is represented by the equation:

$$v = \frac{f_0 - f}{f_0} \cdot c \tag{5}$$

where f_0 is the frequency of the rest frame, f is the frequency and c is the speed of light. Moreover, in order to correct this velocity so that it corresponds to our local frame of reference, a conversion to the local standard of rest must be made. This new velocity (V_{LSR}) gives a velocity that follows the rest frame of the local universe around the Sun. To convert to this velocity, the velocity of the Sun's frame of reference must be taken with respect to the location of the observation. In the case of Eta Carinae, this velocity is estimated to be $V_{LSR,0} \approx -24\, km/s$ (X. Zhang, Lee, et al., 2001). This value can then be added to the velocity-resolved data to convert it to the local standard of rest:

$$V_{LSR} = v + V_{LSR,0}\,. \tag{6}$$

Now, using this equation, the spectra in Sect. 4 can be given in both the IF and the velocity. This velocity now offers a more physical axis to the spectra than the IF. Most importantly, the velocity of an emission or absorption feature can now be determined.

3 Observations

Two GUSTO data sequences will be analysed during this project: sequences 50 and 51. For the entire GUSTO mission, there were a total of around 12000 sequences, meaning that this data was taken in the earliest stages of the mission. As a consequence of this, there were many inconsistencies between sequences. For example, the number of scans per sequence was not the same. Sequence 50 consisted of scanIDs 1459 to 1462, whilst sequence 51 consisted of scanIDs 01463 to 01473. Furthermore, every individual scan was duplicated for both sequences. More of these differences will later be uncovered in this thesis.

This section will go into the theory of the instrumentation used during the observations and discuss the calibration used after the observations.

3.1 GUSTO's Payload

An observatory requires precise and trustworthy instrumentation to observe faint, THz fine-structure lines like [NII] at 1.46 THz. In the case of GUSTO, this was taken into account. Its payload, as stated in Sect. 1, consisted of 5 types of instruments: the telescope, three sets of heterodyne receiver arrays, autocorrelator spectrometers, instrument control electronics and a cryostat. To better understand how these instruments work together when taking data, a diagram for the path of a beam from the telescope was generated (Fig. 5).

Firstly, as light enters the telescope, it is halted by a flip mirror. When flipped, this mirror can redirect the hot load onto the mixers, and when flipped again, the light from the sky enters the mixers. This allows GUSTO to quickly take a hot load measurement during its scans, which is crucial when performing data calibration, as described in Sect. 2.6.

When the flip mirror is not flipped towards the hot load, the beam enters the lenses and is thus focused upon the mixer arrays. These lenses had band-specific parameters, like major axis, minor axis and thickness, that were optimised for the individual band-frequencies (Silva, Laauwen, et al., 2023). Moreover, GUSTO uses hot electron bolometer (HEB) mixers. These were chosen since they can capture these terahertz nitrogen fine-structure lines as discussed in Sect. 2.2.1. These mixers are laid out in a 4×2 array for both the [NII], [CII], and the failed [OI] bands (Fig. 4). This setup allowed for a compact array setup with 8 pixels per band.

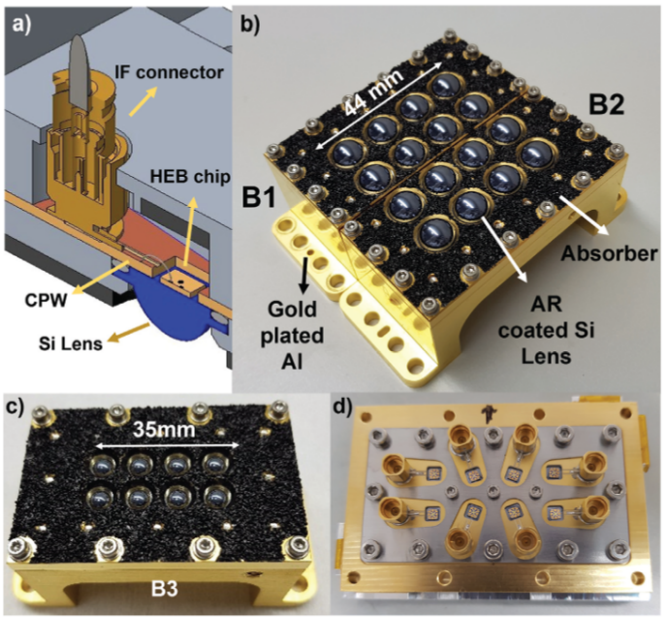

Figure 4: This figure shows the mixer arrays used in the GUSTO observatory. In image a) an overview is given of the individual mixer parts. Image b) shows the 2 arrays of 4×2 HEB mixers. Here, B1 represents the mixers used for the [NII] band, whilst B2 represents the mixers used for the [CII] band. Figure c) shows the failed array for B3, which represents the [OI] band, and image d) shows the backside of a mixer array. (Silva, Laauwen, et al., 2023)

This captured frequency is then mixed with the local oscillator (LO) signal. For the local oscillator (LO) source during the mission, GUSTO used frequency multiplier chain arrays for the [NII] and [CII] bands. In these arrays, the radiation from a local oscillator is combined with the sky radiation from a beam splitter and, after passing through a cryostat window and an infrared heat filter, is coupled to the mixer arrays (Silva, Laauwen, et al., 2023). On the other hand, a quantum cascade laser (QCL) was used for the [OI] band (Silva, Laauwen, et al., 2023). Here, a single QCL beam is multiplexed into multiple beams in a 4×2 pattern by a phase grating, to align with the mixer array (Silva, Laauwen, et al., 2023). The frequency multiplier chain was chosen for bands [NII] and [CII] since their fine-structure line is below 2 THz, thus falling in the frequency range for the LO, and this LO source can operate at room temperature, therefore not requiring cooling. The QCL was chosen as a LO source for the [OI] band since its fine-structure line lies above 2 THz and therefore only falls within the frequency range of the QCL. The frequency multiplier chain LO source choice will potentially create issues for the [CII] and [NII] bands since its output power will be less than that of the QCL LO source, as discussed in Sect. 2.2.2.

Since the mixer and the QCL LO source are required to operate at very low temperatures, a cryostat was used during the mission. This allowed the mixers to operate at a temperature of around $T \sim 4\,K$ and the QCL to operate at a temperature of around $T \sim 40\,K$. Moreover, a temperature of around $T \sim 58\,K$ was used for the cryostat window in the frequency chains.

After mixing, a new intermediate frequency (IF) was formed. This signal was then amplified by a low-noise amplifier (LNA), followed by filtering for noise, and finally processing of the signal by the IF processor and the spectrometer. This processed signal is stored within GUSTO's instrument and gondola computers and downlinked to the ground station at specific frequencies. Due to these particular downlink frequencies, spurs are found within

the data, meaning that the spectra at these frequencies have an extraordinarily high or low peak as the instruments capture these frequencies. Therefore, at these frequencies, the spectra become unreadable and thus unusable.

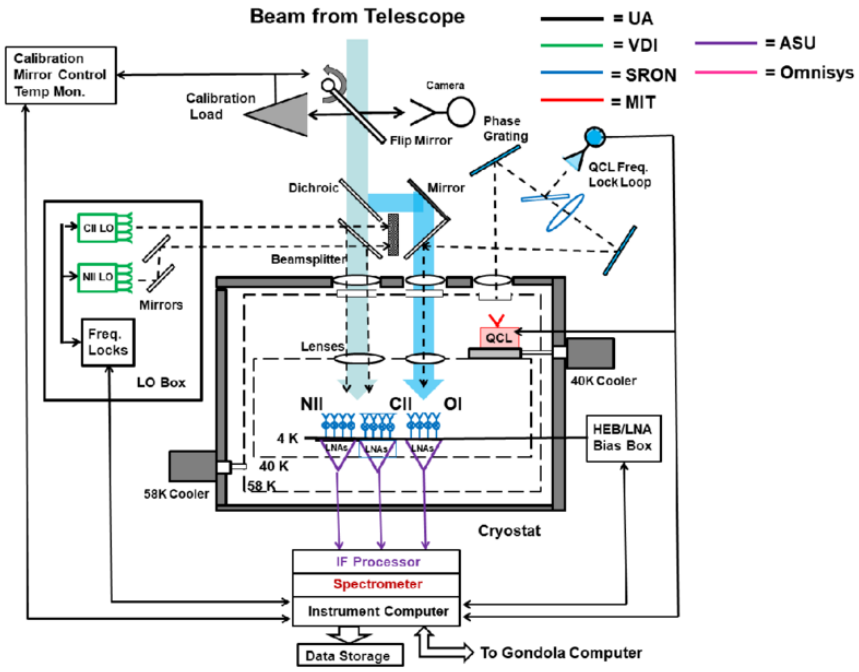

Figure 5: Diagram showing the instruments within the GUSTO gondola. Moreover, it shows the path that the beam takes as it enters the heterodyne receiver. (Walker, Kulesa, et al., 2022)

3.2 Calibration of GUSTO's Data

The y-factor method, as discussed in Sect. 2.6 is used to create spectra for the raw data obtained from the GUSTO mission. For the GUSTO mission, this method was then slightly adapted. This was done by taking both on-source and off-source (reference) measurements to provide clearer calibration. Both of these measurements came with a respective hot source measurement. Using this method, a y-factor could be generated using the reference points:

$$Y = \frac{P_{ref,hot}}{P_{ref}} \tag{7}$$

where $P_{ref,hot}$ is the measured power of the hot source at the reference position and P_{ref} is the measured power of the reference point on the sky. Using this equation and applying it to every frequency, the y-factor could be plotted (Fig. 6).

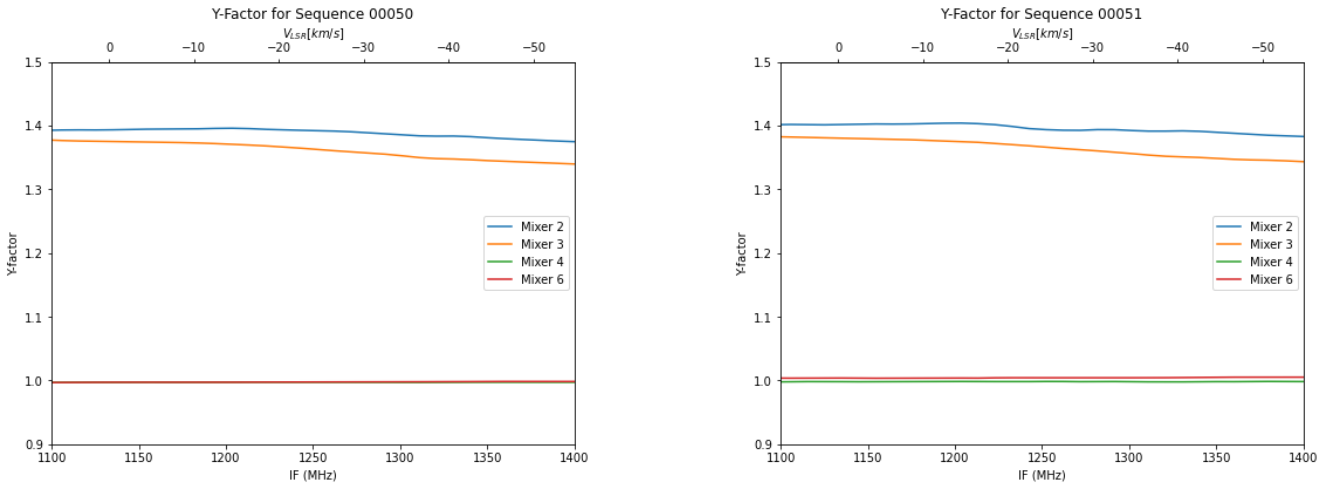

(a) (b)

Figure 6: Figures showing the values of the y-factor with respect to the IF for a) Sequence 50 and b) Sequence 51. The blue plot represents mixer 2, the orange plot represents mixer 3, and the red and green plots respectively represent mixers 4 and 6. Note that in sequence 50, both mixers 4 and 6 have a constant y-factor of near 1.

Here, in both sequences 50 and 51, mixer 2 has a y-factor of around $Y \approx 1.4$, mixer 3 has a y-factor of around $Y \approx 1.37$, and both mixers 4 and 6 have a y-factor of 1. Since a low y-factor indicates a noisy spectrum, mixers 4 and 6 will have noise in the spectra for both sequences 50 and 51, which makes sense since these mixers did not work correctly and thus provided poor spectra. On the other hand, the higher y-factor for mixers 2 and 3 indicates clear spectra for these mixers.

These y-factors could then be applied to equation 3 to create the noise temperature. For the variables in this equation, T_{sky}, after applying equation 4, was found to be $T_{sky} = 35.06\,K$ and T_{hot} after measurements by GUSTO temperature monitor, was found to be $T_{hot} \approx 284\,K$ for both sequences 50 and 51.

A spectrum could be generated after obtaining both the y-factor and the noise temperature. This is achieved by obtaining a ratio of the power measured from the difference between the source and a synthetic reference, and dividing it by the measured reference. Here, a synthetic reference can be determined by dividing the measured power of the hot during a source measurement by the y-factor. Consequently, by using this principle, the following formula is obtained:

$$T_A = T_N \cdot \frac{P_{src} - \frac{P_{src,hot}}{Y}}{P_{ref}} \tag{8}$$

where T_N is the noise temperature, P_{src} is the measured power of the source, $P_{src,hot}$ is the measured power of the hot during the source measurement, P_{ref} is the measured power of the reference on the sky and Y is the y-factor. In sequence 50, this noise temperature averaged over the entire spectrum was $T_N = 787.15\,K$ for mixer 2 and $852.22\,K$ for mixer 3. In sequence 51, the averaged noise temperature for mixer 2 was $T_N = 802.21\,K$ and for mixer 3 $T_N = 877.08\,K$. Now, the spectra could be obtained.

3.2.1 Mixer Offsets

As shown in Sect. 4, the raw pointing data extracted from the GUSTO mission must also be calibrated to generate accurate positional maps for the scans per sequence. Thus, a mixer offset must be applied to account for the positional differences between the mixers. This offset is based on the distance between the mixers and the boresight. During the GUSTO mission, the boresight was defined to be mixer 8 from the [CII] band (Fig. 7). A theoretical offset could be determined using the positional differences between the mixers and the boresight (Tab. 2). After extracting the raw pointing data of the gondola for the [NII] band, the offsets could be summed with the raw positions to form the correctly calibrated pointing per mixer.

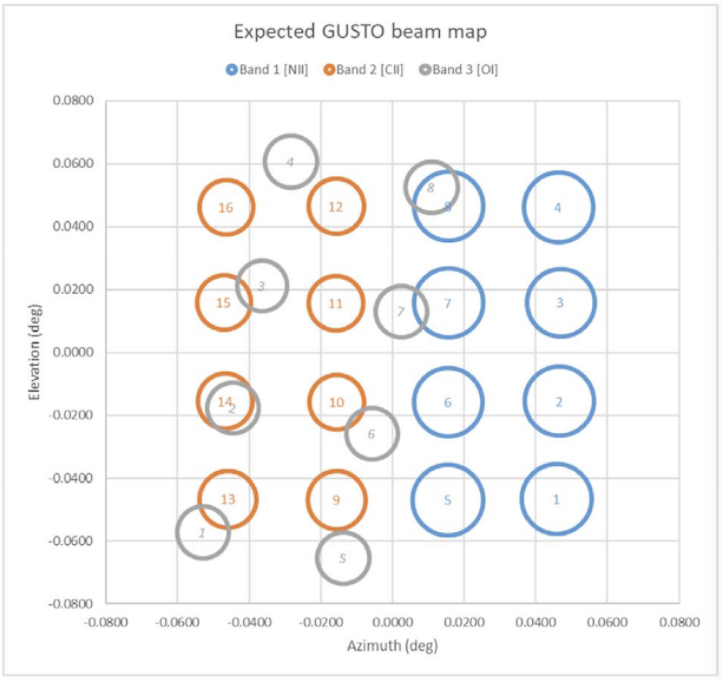

Figure 7: Figure showing the position and beam-size of GUSTO's mixers for the [CII] band (Orange), the [NII] band (Blue) and the failed [OI] band (Grey). Important to note is that the mixer labelling used in this figure differs from the labelling found in the GUSTO data. For example, for the working mixers in the [NII] band, the mixers labelled 5 and 2 actually represent mixers 2 and 3.

Mixer	Azimuth Offset (degrees)	Altitude Offset (degrees)
1	0.061273	0.000406
2	0.091139	-0.000226
3	0.060790	-0.030935
4	0.093381	-0.032414
5	0.062584	-0.062968
6	0.092809	-0.063639
7	0.060754	-0.094123
8	0.093356	-0.093330

Table 2: Theoretical offsets of the 8 mixers in the [NII] mixer array. The offsets are relative to the bore sight, defined as the 8th mixer in the [CII] array, represented by mixer 9 in Fig. 7.

4 Results

After applying the theory discussed in Sect. 2, spectra could be formed. These spectra were created for only mixers 2 and 3. This is because mixers 4 and 6 gave extremely noisy spectra, indicating that something went wrong during the observations for these mixers. Moreover, the positions of the scans and the type of measurements needed to be analysed to clarify what the mixers were pointing at. In the case of [NII], each of these measurements was taken with a spatial resolution of around 0.9 arcminutes (Walker, Kulesa, et al., 2022). The positions of the scans are significant regarding spectra calibration, since the calibration must remain consistent. Thus, after accounting for these factors, spectra could be generated for sequences 50 and 51 for mixers 2 and 3.

4.1 Sequence 50

Sequence 50 for both mixers 2 and 3 consisted of 16 source measurements on the target of Eta Carinae 5, 12 source-hot measurements taken on the hot load close in time with respect to the target, 12 reference measurements

taken on the blank sky and 12 reference-hot measurements, taken on the hot source close in time after a reference measurement. Thus, there was a total of 52 measurements. These ran from 11:48:24 to 11:50:22, for a total of 118 seconds, on the 11th of January 2024. After extracting the positions of the scans, maps could be formed for both mixers 2 and 3 (Fig. 8). This figure shows that for both mixers, the data taken in this sequence were located at 2 different positions, separated by a distance of around 20.3 arcminutes. When looking at the upper position in this map (Fig. 15), only reference measurements and reference-hot measurements are found. Thus, this upper position does not contain any source or source-hot measurements. When looking at the lower position in this map (Fig. 15), all 4 types of measurements are found. Thus, contrary to the upper position, this lower position contains source and source-hot measurements. To perform accurate calibration, the lower reference and reference-hot measurements were ignored, since these were taken at the same position as the source and at a different position from the other reference and reference-hot measurements.

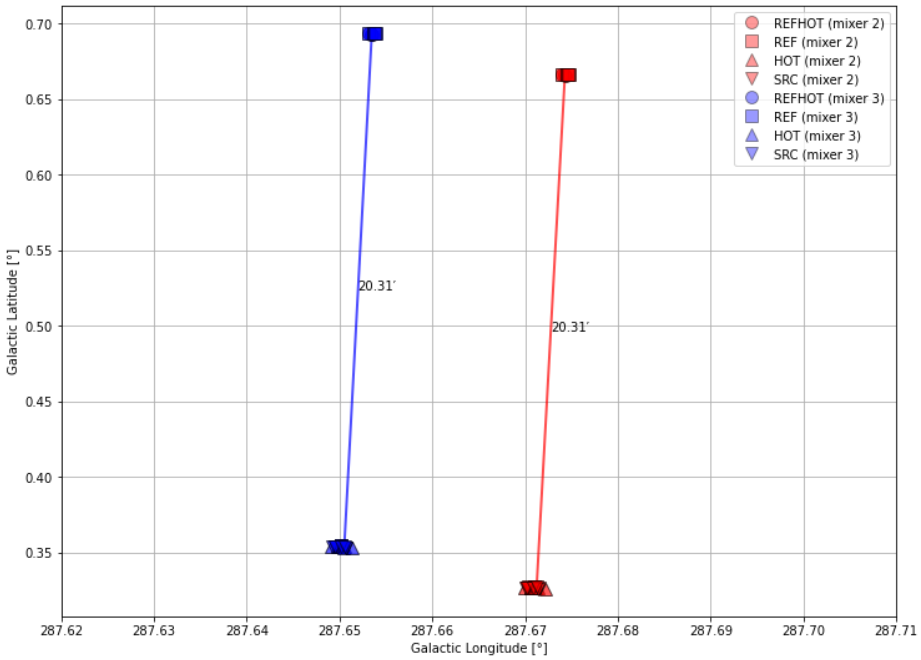

Figure 8: Figure showing the positions and measurement types for the scans in sequence 50 for mixer 2 (Red) and mixer 3 (Blue). These measurements include a source measurement on the target (Nabla), a source-hot measurement integrated on the hot load close in time with respect to the source measurement (Triangle), a reference measurement taken on the blank sky (Square) and a reference-hot measurement (Circle) integrated of the hot load close in time after a reference measurement. In the case of no motion of the gondola occurring, both source and source-hot, as well as reference and reference-hot measurements, should be at the same location. The distance between the two positions for mixers 2 and 3 is around 20.31 arcminutes. A more detailed view of the measurements at each position can be seen in Figure 15.

After filtering the reference and reference-hot measurements, a spectrum could be generated for the source positions, located at the galactic coordinates $(287.67°, 0.33°)$ for mixer 2 (Fig. 9a) and $(287.65°, 0.35°)$ mixer 3 (Fig. 9b).

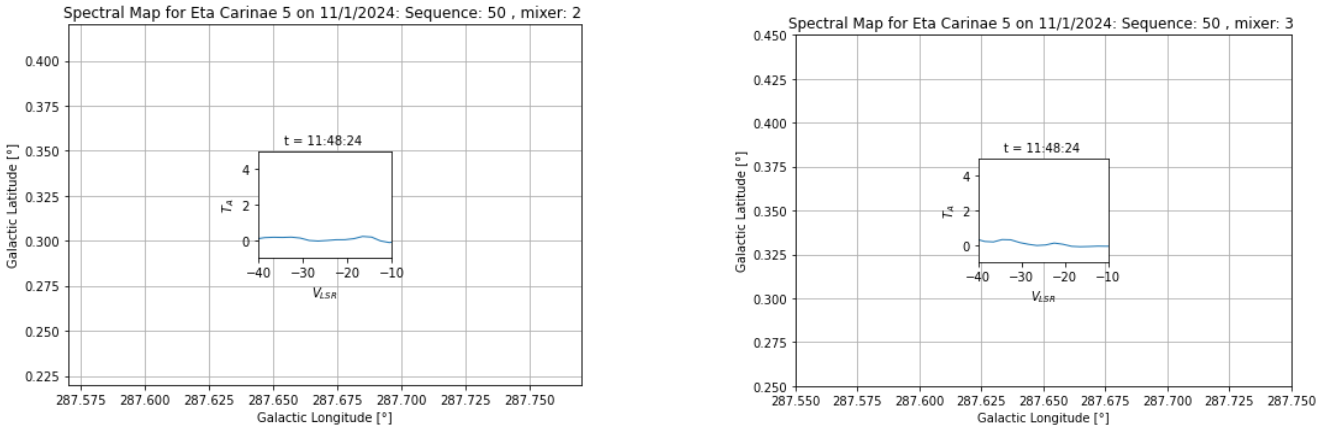

(a) (b)

Figure 9: Figure containing the spectra in sequence 50 for mixers a) 2 and b) 3 with respect to their position in galactic coordinates. Above each of these spectra, the start time of the observation at that position is given. Due to the velocity of the region being around -20 km/s, as stated in Sect. 2.7, the velocity axis was limited between -40 and 0 km/s.

4.2 Sequence 51

In the case of sequence 51 for the mixers 2 and 3, there were a total of 44 source measurements, 60 source-hot measurements and 6 reference-hot measurements. Yet, mixer 2 consisted of 2 reference measurements, whilst mixer 3 consisted of 4 reference measurements. Therefore, mixers 2 and 3 contained 112 and 114 measurements, respectively. These ran on the same date as sequence 50: 11th of January 2024, over a timespan of 11:50:26 to 11:57:04 for 6 minutes and 38 seconds. Unlike sequence 50, where the scans were taken at two positions, this sequence consisted of a 16×16 arcminute grid of 9 scans (Fig. 10). The first scan started at the centre of the grid, where every proceeding positional switch spirals around this central point.

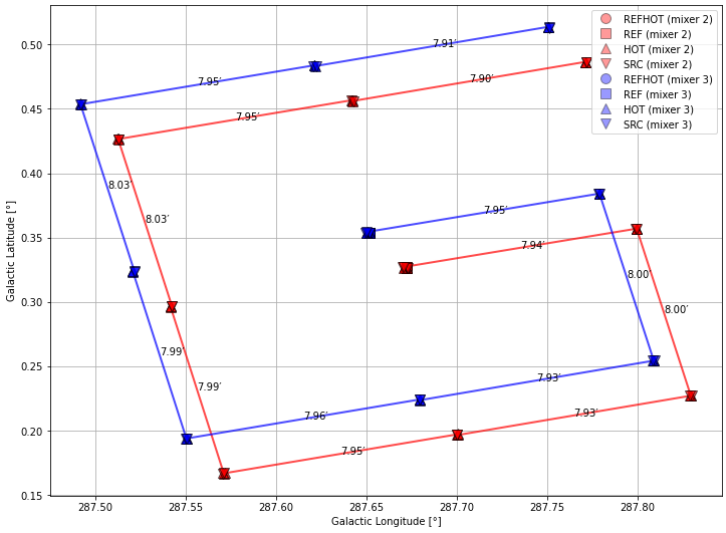

Figure 10: Figure showing the positions and measurement types for the scans in sequence 51 for mixer 2 (Red) and mixer 3 (Blue). These measurements include a source measurement on the target (Nabla), a source-hot measurement integrated on the hot load close in time with respect to the source measurement (Triangle), a reference measurement taken on the blank sky (Square) and a reference-hot measurement (Circle) integrated of the hot load close in time after a reference measurement. For both mixers, only reference and reference-hot measurements were taken at the central scan, with the other positions just being source positions. The distance between every positional shift is given in arcminutes. A more detailed view of the central position can be seen in Figure 16 and a timeline of the positional shifts in Table 3.

Within this grid, all 9 positions contained both source and source-hot measurements. Therefore, all 9 positions could be taken as source positions, and a spectrum could be formed for these positions. However, only the central position within the grid contained reference and reference-hot measurements. Since this position also contained source measurements, it could be considered as both a reference and source position (Tab. 3). When using the central position in sequence 51 as both a source and reference position, a Gaussian-shaped emission feature is found within all 9 plots (Fig. 11a). On the other hand, when looking at mixer 3, this peak cannot be found (Fig. 11b).

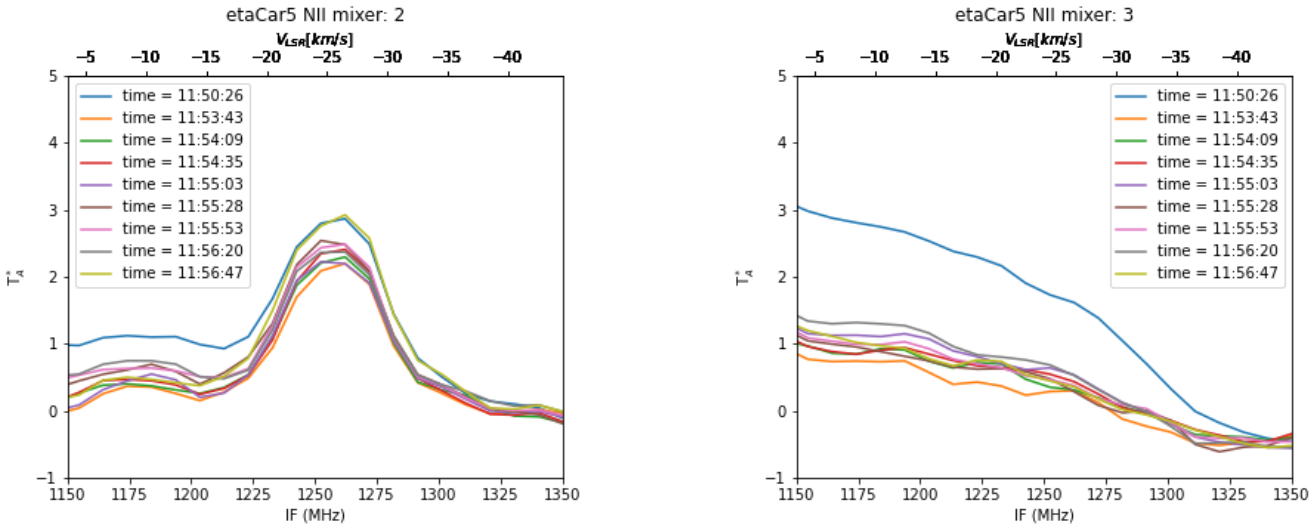

(a) (b)

Figure 11: Figure containing the spectra in sequence 51 for mixers a) 2 and b) 3 for every starting time, based upon the positions in Figure 10. These spectra are given in more IF and velocity. Due to the velocity of the region being around -20 km/s, the velocity axis was limited between -40 and 0 km/s.

However, when again using the source and source-hot measurements for each point in the grid, but now using the upper position containing the reference and reference-hot measurements of sequence 50 as the reference position in this sequence, a new grid of spectral maps was formed for mixer 2 (Fig. 12) and for mixer 3 (Fig. 13), where this apparent peak disappears, showing a flat spectrum for both mixers. Using the reference position in sequence 50, a position where, according to Sect. 4.2, there certainly is not a source; the reference position in sequence 51 could be tested.

Position	Position type	Observation Start Time	Mixer 2: (l, b) (degrees)	Mixer 3: (l, b) (degrees)
1	Reference and Source	11:50:26	(287.67, 0.32)	(287.64, 0.35)
2	Source	11:53:43	(287.79, 0.35)	(287.77, 0.38)
3	Source	11:54:09	(287.82, 0.22)	(287.80, 0.25)
4	Source	11:54:35	(287.70, 0.19)	(287.67, 0.22)
5	Source	11:55:03	(287.57, 0.16)	(287.55, 0.19)
6	Source	11:55:28	(287.54, 0.29)	(287.52, 0.32)
7	Source	11:55:53	(287.51, 0.42)	(287.49, 0.45)
8	Source	11:56:20	(287.64, 0.45)	(287.62, 0.48)
9	Source	11:56:47	(287.77, 0.48)	(287.75, 0.51)

Table 3: Table showing information on the 9 positions in the 16×16 arcminute grid in sequence 51. This table gives the position type, the observation start time, and the galactic coordinates for both mixers 2 and 3 at every of the 9 positions.

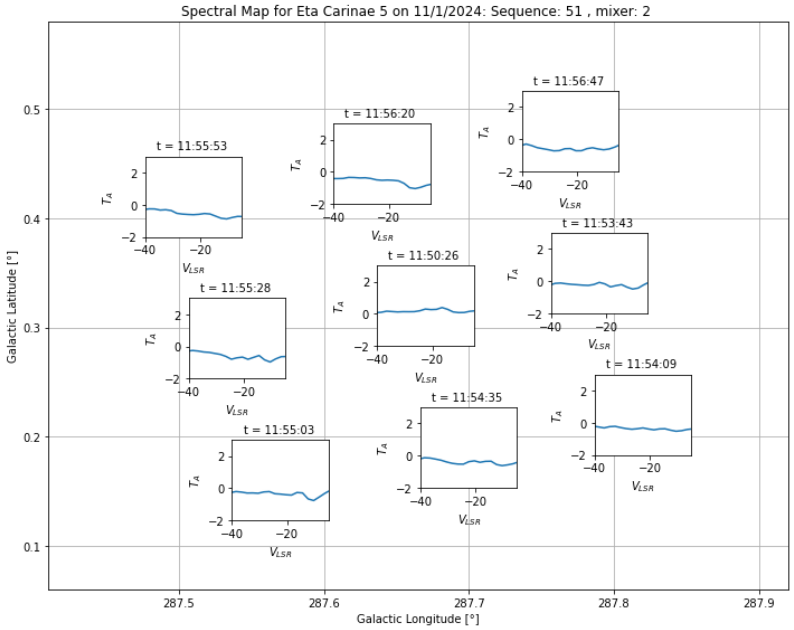

Figure 12: Figure containing the 9 spectral plots for the source positions of mixer 2 in sequence 51 with respect to the scan positions in galactic coordinates. Above each of these 9 spectra, the start time of the observation at that position is given. Instead of using the reference position in sequence 51, these plots used the reference position in sequence 50 during their calibration. Due to the velocity of the gas in the region being around -20 km/s, as stated in Sect. 2.7, the velocity axis was limited between -40 and 0 km/s.

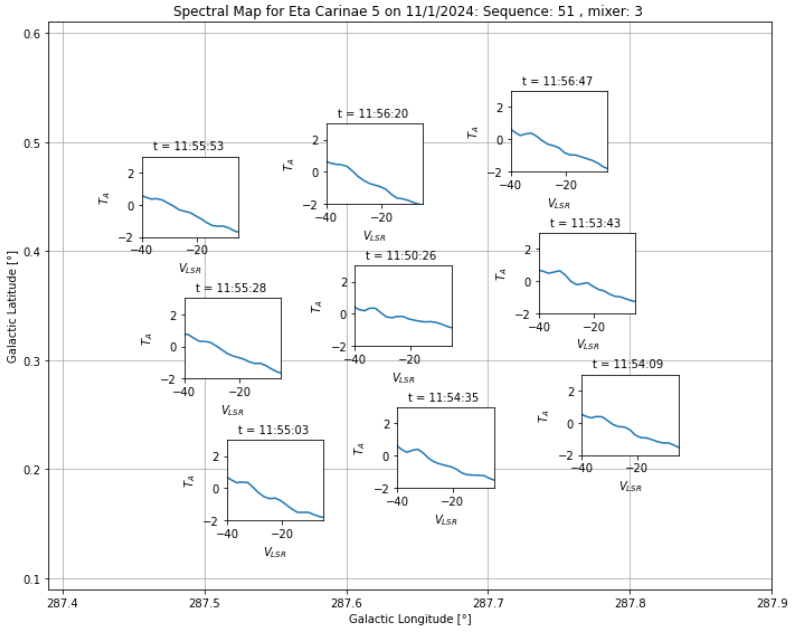

Figure 13: Figure containing the 9 spectral plots for the source positions of mixer 3 in sequence 51 with respect to the scan positions in galactic coordinates. Above each of these 9 spectra, the start time of the observation at that position is given. Instead of using the reference position in sequence 51, these plots used the reference position in sequence 50 during their calibration. Due to the velocity of the gas in the region being around -20 km/s, as stated in Sect. 2.7, the velocity axis was limited between -40 and 0 km/s.

5 Discussion

When looking at the observation types for sequences 50 and 51, both are Position Switch (PS) observations. In the case of sequence 50 for mixers 2 and 3, this position shift consisted of 2 positions, separated by 20.31 arcminutes, located at around the same longitude with a varying latitude (Fig. 8). Here, the upper latitude position contained only reference and reference-hot measurements, thus making it the reference position in this sequence (Fig. 15). At the lower altitude position, mostly source and source-hot measurements were found, making it the source position (Fig. 15). This made sequence 50 a standard PS observation, since only a single reference and a source position were present in this sequence.

On the other hand, sequence 51 consisted of a 16×16 arcminute grid of 9 positions. Here, only the central position contained a reference and reference-hot measurement, whilst the other 8 points only had source and source-hot measurements (Fig. 10). Thus, this sequence contained 1 reference position and 8 source positions. However, the central position in the sequence, aside from reference and reference-hot measurements, also contained source and source-hot measurements (Fig. 16). This central point was therefore taken as both a source and reference position, resulting in a total of 1 reference position and 9 source positions in this sequence. Due to this PS observation containing 9 positions, this sequence is somewhat non-standard. This is probably the case since during this sequence, GUSTO was trying to figure out where it was in the sky. Using this 9-point PS observation allowed it to test its point whilst simultaneously performing calibratable observations.

Moreover, for mixer 2 in sequence 51, an emission feature is seen when using the reference position in the sequence, showing a clear Gaussian peak for all source positions (Fig. 11a). This feature, therefore, indicates the supposed presence of [NII] within all 9 source positions. However, this feature should not be present for the position that was taken as both a reference and a source position. This is because the measurements at this position should be the same, and consequently, when applying the calibration in Sect. 3.2, a blank spectrum should appear. Additionally, in mixer 3 this feature does not appear for any of the 9 source positions (Fig. 11b). This again does not make sense, since these mixers observe the same region with a slight offset from each other. Therefore, some of the source positions in mixer 3 would still take scans of the same region in mixer 2. Consequently, there must be an error in either the source measurements at this central position or the reference measurements of the entire sequence in the case of mixer 2.

To further test this, the reference position from sequence 50 was taken. Here, in all 9 of the source positions, no [NII] emission peaks were present (Fig. 12, 13). Since the reference position in sequence 50 does not contain a source, it can be assumed that this error must be present in the reference measurements of sequence 51 in mixer 2. This is most likely the effect of a spur present during the reference measurements. In mixer 2, these reference measurements occurred over a timespan of 2.1 seconds, where 1 measurement was duplicated. This must have tainted the reference measurements of mixer 2 in sequence 51, resulting in a noticeable artefact within the data. This random spur might have occurred due to the local oscillator. This is because at higher power levels, the chance that a spur might happen in the local oscillator (LO) increases, due to the LO diodes having a worse-controlled transconductance at high power levels (Marki & Marki, 2010). This means that the current flow and voltage ratio can become unstable.

Moreover, the positions of the scans found in the data are far away from the actual position of Eta Carinae 5 (Fig. 14). This issue is probably due to an error in the initial coordinates found by the star-tracker. Additionally, the catalogue used during the GUSTO mission states that GUSTO was indeed pointing towards Eta Carinae 5 during these sequences. Since this catalogue is directly controlled and maintained by the GUSTO team, it can be assumed that it is correct. Yet, whilst we can assume that GUSTO was looking at Eta Carinae 5 during sequences 50 and 51, it cannot be concluded that this is true.

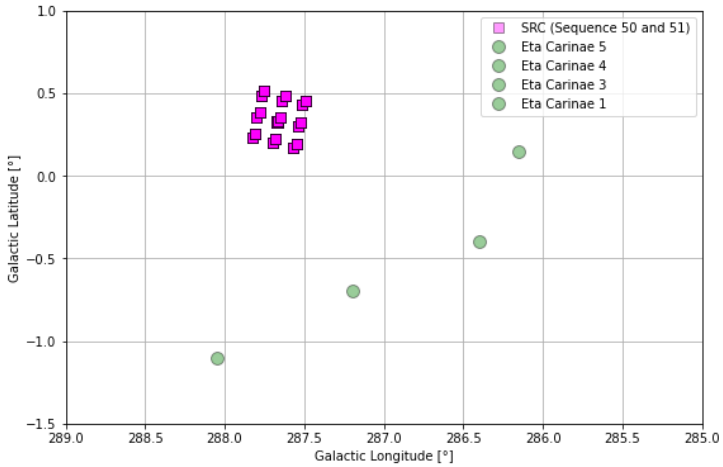

Figure 14: Figure showing both the galactic coordinates of the source positions found in sequences 50 and 51 for mixers 2 and 3 (Purple Squares), and the centre of Eta Carinae regions 1, 3, 4, and 5 (Green Circles), as defined by Zhang (X. Zhang, Lee, et al., 2001).

Aside from this, the lack of emission peaks indicates that no [NII] emission was present in the regions scanned by GUSTO in sequences 50 and 51. This is not a surprising result, since the purpose of GUSTO pointing at Eta Carinae 5 was not to find [NII], but to figure out its pointing. Furthermore, [NII] emission is difficult and rare to detect. Due to the positional errors within the sequences, it is tough to prove whether there might be [NII] emission present, since it is unknown where GUSTO was exactly looking.

6 Conclusions

The initial phases of the GUSTO mission contained many inconsistencies. These are found within the observation types, where varying types of Position Switch (PS) observations were used in the early phases of the GUSTO mission. Sequencing 50 had 2 scan positions, 1 reference and 1 source separated by 20.31 arcminutes, making it a standard PS scan. On the other hand, sequence 51 had a total of 9 scan positions, 8 source positions and a central source and reference position, formed in a 16 arcminute by 16 arcminute grid, making it somewhat non-standard since in this sequence, GUSTO was trying to test its pointing. Moreover, the number of scans for the sequences was inconsistent, where sequence 51 consisted of more scans than sequence 50. Aside from this, when looking at the spectra formed in the source positions for both sequences 50 and 51, no [NII] emission features were found.

To improve the initial measurements of GUSTO, its sequences should be more consistent. This includes explaining the positions of the scans to avoid confusion during calibration. Moreover, there should be an even divide between the 4 scan types. For example, in sequence 51 for mixer 2, there was only a single duplicated reference measurement, resulting in the artefact within these measurements becoming more pronounced in the sequence. Additionally, many of the source and reference measurements were taken at the same position, which defeats the purpose of a reference position. Therefore, these scans should be taken while considering the calibration of the data.

Regarding the [NII] emission, the odds of finding the feature would increase if more mixers were available. Out of the 8 mixers, only mixers 2 and 3 gave working spectra. Thus, if more mixers were working or present, more of the Eta Carinae 5 region could be scanned, increasing the chance of finding the [NII] fine-structure line.

7 References

A. Kramida, Yu. Ralchenko, J. Reader, & and NIST ASD Team. (2024).

Betz, A. L., Boreiko, R. T., Williams, B. S., Kumar, S., Hu, Q., & Reno, J. L. (2006). The quantum cascade laser as a terahertz local oscillator.

de Graauw, T., Helmich, F. P., Phillips, T. G., Stutzki, J., Caux, E., Whyborn, N. D., Dieleman, P., Roelfsema, P. R., Aarts, H., Assendorp, R., Bachiller, R., Baechtold, W., Barcia, A., Beintema, D. A., Belitsky, V., Benz, A. O., Bieber, R., Boogert, A., Borys, C., ... Zwart, F. (2010). Theherschel-heterodyne instrument for the far-infrared (hifi). *Astronomy and Astrophysics*, *518*, L6. https://doi.org/10.1051/0004-6361/201014698

Draine, B. T. (2011). *Physics of the interstellar and intergalactic medium.* Princeton University Press.

Griffiths, D. J., & Schroeter, D. F. (2024). *Introduction to quantum mechanics.* Cambridge University Press.

Heyminck, S., Graf, U. U., Güsten, R., Stutzki, J., Hübers, H. W., & Hartogh, P. (2012). Great: The sofia high-frequency heterodyne instrument. *Astronomy &; Astrophysics*, *542*, L1. https://doi.org/10.1051/0004-6361/201218811

Kerr, A. R., & Randa, J. (2010). *Thermal noise and noise measurements - a 2010 update.* IEEE Microwave Magazine.

Kramer, C., Cubick, M., Röllig, M., Sun, K., Yonekura, Y., Aravena, M., Bensch, F., Bertoldi, F., Bronfman, L., Fujishita, M., Fukui, Y., Graf, U. U., Hitschfeld, M., Honingh, N., Ito, S., Jakob, H., Jacobs, K., Klein, U., Koo, B.-C., ... Yamamoto, H. (2007). Clumpy photon-dominated regions in carina: I. [c i] and mid-jco lines in two 4'×4' fields. *Astronomy amp; Astrophysics*, *477*(2), 547–555. https://doi.org/10.1051/0004-6361:20077815

Lin, Y.-J., & Jarrahi, M. (2020). Heterodyne terahertz detection through electronic and optoelectronic mixers. *Reports on Progress in Physics*, *83*(6), 066101. https://doi.org/10.1088/1361-6633/ab82f6

Marki, F., & Marki, C. (2010). *Mixer basics primer: A tutorial for rf microwave mixers.* Marki microwave.

Mehdi, I., Siles, J. V., Lee, C., & Schlecht, E. (2017). Thz diode technology: Status, prospects, and applications. *Proceedings of the IEEE*, *105*(6), 990–1007. https://doi.org/10.1109/jproc.2017.2650235

NASA. (2015). Sto-2/gusto/lbr: New windows into our cosmic origins [[Accessed 20-06-2025]].

Persson, C. M., Gerin, M., Mookerjea, B., Black, J. H., Olberg, M., Goicoechea, J. R., Hassel, G. E., Falgarone, E., Levrier, F., Menten, K. M., & Pety, J. (2014). First detection of [n ii] 205m absorption in interstellar gas: Herschel-hifi observations towards w31c, w49n, w51, and g34.3+0.1. *Astronomy &; Astrophysics*, *568*, A37. https://doi.org/10.1051/0004-6361/201423997

Physical Research Laboratory. (2007). Schottky Mixer — prl.res.in [[Accessed 21-06-2025]].

Richards, P. L. (1994). Bolometers for infrared and millimeter waves. *Journal of Applied Physics*, *76*(1), 1–24. https://doi.org/10.1063/1.357128

Richter, H., Greiner-Bär, M., Günther, B., Rösner, K., & Hübers, H.-W. (2010, March). A 4.7-thz gas laser local oscillator for great on sofia.

Seo, Y. M., Goldsmith, P. F., Walker, C. K., Hollenbach, D. J., Wolfire, M. G., Kulesa, C. A., Tolls, V., Bernasconi, P. N., Kavak, Ü., van der Tak, F. F. S., Shipman, R., Gao, J. R., Tielens, A., Burton, M. G., Yorke, H., Young, E., Peters, W. L., Young, A., Groppi, C., ... Kuiper, T. B. (2019). Probing ism structure in trumpler 14 and carina i using the stratospheric terahertz observatory 2. *The Astrophysical Journal*, *878*(2), 120. https://doi.org/10.3847/1538-4357/ab2043

Silva, J. R. G., Laauwen, W. M., Mirzaei, B., Vercruyssen, N., Finkel, M., Westerveld, M., More, N., Silva, V., Young, A., Kulesa, C., Walker, C., van der Tak, F., & Gao, J. R. (2023). 4x2 hot electron bolometer mixer arrays for detection at 1.46, 1.9 and 4.7 thz for a balloon borne terahertz observatory. https://doi.org/10.48550/ARXIV.2311.05755

SIMBAD. (2025). Eta car [[Accessed 20-06-2025]].

Smith, D. (2025). Explorers Program — explorers.gsfc.nasa.gov [[Accessed 20-06-2025]]. https://explorers.gsfc.nasa.gov/unex_mo_intern.html#gusto

SRON. (2025). GUSTO - SRON | Space Research Organisation Netherlands — sron.nl [[Accessed 20-06-2025]]. https://www.sron.nl/en/missions/active/gusto/

Steinmassl, S., Breuhaus, M., White, R., Reville, B., & Hinton, J. A. (2023). Probing cosmic ray escape from eta carinae. *Astronomy &; Astrophysics*, *679*, A118. https://doi.org/10.1051/0004-6361/202346483

Thomas L. Wilson, S. H., Kristen Rohlfs. (2009). *Tools of radio astronomy.* Astronomy & Astrophysics Library.

Walker, C. K., Kulesa, C. A., Young, A., Verts, W., Gao, J.-R., Hu, Q., Silva, J. R., Mirzaei, B., Laauwen, W., Hesler, J. L., Groppi, C., & Emrich, A. (2022, August). Gal/xgal u/ldb spectroscopic/stratospheric thz observatory: Gusto. In J. Zmuidzinas & J.-R. Gao (Eds.), *Millimeter, submillimeter, and far-infrared detectors and instrumentation for astronomy xi* (p. 22). SPIE. https://doi.org/10.1117/12.2629051

Zhang, W., Miao, W., Ren, Y., Zhou, K.-M., & Shi, S.-C. (2022). Superconducting hot-electron bolometer mixers and their applications. *Superconductivity*, *2*, 100009. https://doi.org/10.1016/j.supcon.2022.100009

Zhang, X., Lee, Y., Bolatto, A., & Stark, A. A. (2001). Co (j=4→3) and [ci] observations of the carina molecular cloud complex. *The Astrophysical Journal*, *553*(1), 274–287. https://doi.org/10.1086/320628

8 Appendix

8.1 Appendix A: Code

The code used during the data reduction of this thesis can be found by opening the following link: https://drive.google.com/file/d/1qTsvHgvV8n4EI75sj1cuBhHGJgw_b7aU/view?usp=sharing

8.2 Appendix B: Figures

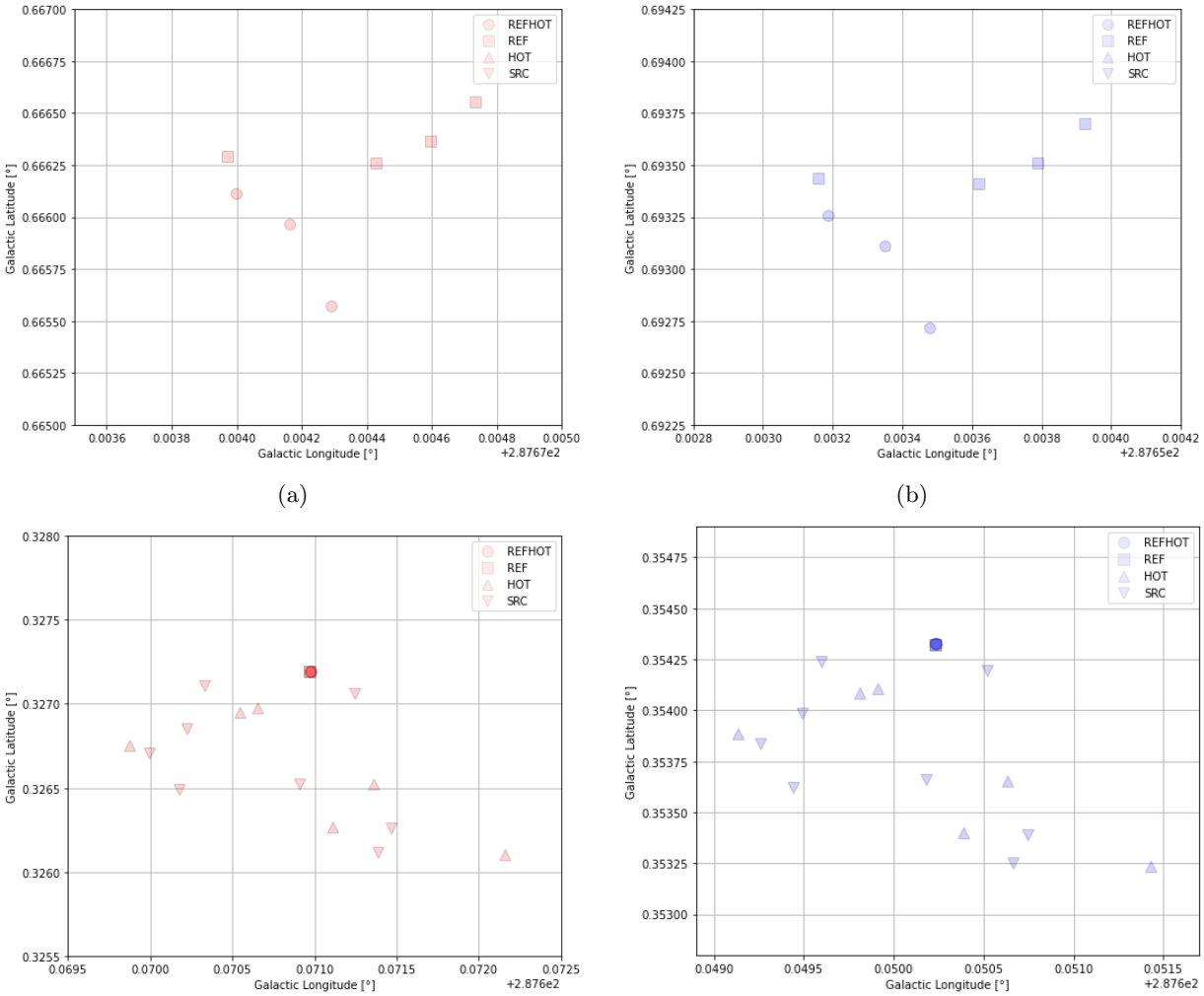

(a) (b) (c) (d)

Figure 15: Figures showing a detailed view of the 2 scan positions in sequence 50 for mixers 2 (Red) and 3 (Blue), as shown in Figure 8. This includes the higher altitude position for a) mixer 2 and b) mixer 3, and the lower altitude position for c) mixer 2 and d) mixer 3. These measurements include a source measurement on the target (Nabla), a source-hot measurement integrated on the hot load close in time with respect to the source measurement (Triangle), a reference measurement taken on the blank sky (Square) and a reference-hot measurement (Circle) integrated of the hot load close in time after a reference measurement. Important to note is that the reference-hot measurements are hard to see in sub-figures 15c and 15d, yet they are present, since they are taken at the same position as the reference measurement.

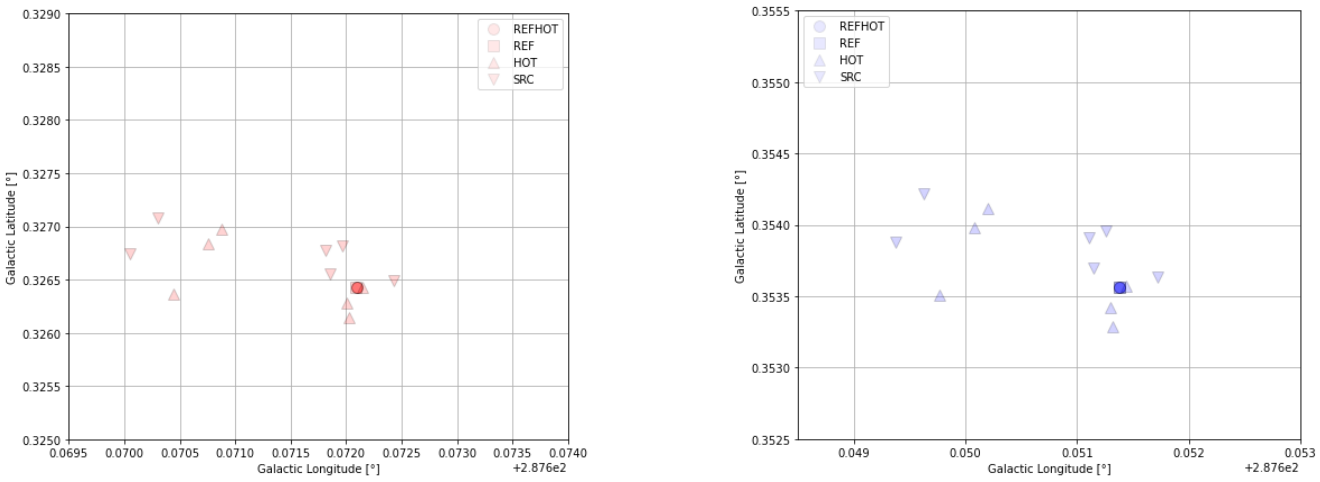

(a) (b)

Figure 16: Figures showing a detailed view of the central scan position in sequence 51 for mixers a) 2 (Red) and b) 3 (Blue), as shown in Figure 10. These measurements include a source measurement on the target (Nabla), a source-hot measurement integrated on the hot load close in time with respect to the source measurement (Triangle), a reference measurement taken on the blank sky (Square) and a reference-hot measurement (Circle) integrated of the hot load close in time after a reference measurement. For both sub-figures 16a and 16b, both the reference and the reference hot measurements are taken at the same position, with a source-hot measurement right next to it.

8.3 Appendix C: Tables

Mixer	Observation Date and Time	Scan Type	Galactic Longitude	Galactic Latitude	Integration Time
2	2024-01-11T11:48:24.813	REFHOT	287.67097858210764	0.327195144979327	2.166712
2	2024-01-11T11:48:24.813	REFHOT	287.67097858210764	0.327195144979327	2.166712
2	2024-01-11T11:48:26.979	REFHOT	287.6709768525084	0.3271949489004839	2.166712
2	2024-01-11T11:48:26.979	REFHOT	287.6709768525084	0.3271949489004839	2.166712
2	2024-01-11T11:48:29.146	REFHOT	287.67097512204623	0.32719475303606116	2.166712
2	2024-01-11T11:48:29.146	REFHOT	287.67097512204623	0.32719475303606116	2.166712
2	2024-01-11T11:48:33.721	REF	287.6709714684597	0.32719434052617924	2.166712
2	2024-01-11T11:48:33.721	REF	287.6709714684597	0.32719434052617924	2.166712
2	2024-01-11T11:48:35.887	REF	287.6709697385962	0.327194145700673	2.166712
2	2024-01-11T11:48:35.887	REF	287.6709697385962	0.327194145700673	2.166712
2	2024-01-11T11:48:51.000	HOT	287.6698720073276	0.32675606282468167	2.166712
2	2024-01-11T11:48:51.000	HOT	287.6698720073276	0.32675606282468167	2.166712
2	2024-01-11T11:48:53.166	HOT	287.6705463145493	0.3269538221643114	2.166712
2	2024-01-11T11:48:53.166	HOT	287.6705463145493	0.3269538221643114	2.166712
2	2024-01-11T11:48:55.333	HOT	287.6706514369116	0.3269772790376721	2.166712
2	2024-01-11T11:48:55.333	HOT	287.6706514369116	0.3269772790376721	2.166712
2	2024-01-11T11:49:00.207	SRC	287.6702262068353	0.3268546925555265	2.166712
2	2024-01-11T11:49:00.207	SRC	287.6702262068353	0.3268546925555265	2.166712
2	2024-01-11T11:49:02.373	SRC	287.6703329806832	0.327108832634131	2.166712
2	2024-01-11T11:49:02.373	SRC	287.6703329806832	0.327108832634131	2.166712
2	2024-01-11T11:49:04.540	SRC	287.6699957815089	0.3267083358688681	2.166712
2	2024-01-11T11:49:04.540	SRC	287.6699957815089	0.3267083358688681	2.166712
2	2024-01-11T11:49:06.707	SRC	287.6701745062959	0.3264933850484799	2.166712
2	2024-01-11T11:49:06.707	SRC	287.6701745062959	0.3264933850484799	2.166712
2	2024-01-11T11:49:32.383	HOT	287.6713590904991	0.3265212261776563	2.166712
2	2024-01-11T11:49:32.383	HOT	287.6713590904991	0.3265212261776563	2.166712
2	2024-01-11T11:49:34.549	HOT	287.67111393627135	0.3262671117554675	2.166712
2	2024-01-11T11:49:34.549	HOT	287.67111393627135	0.3262671117554675	2.166712
2	2024-01-11T11:49:36.716	HOT	287.6721558577898	0.3261000253641977	2.166712
2	2024-01-11T11:49:36.716	HOT	287.6721558577898	0.3261000253641977	2.166712
2	2024-01-11T11:49:41.496	SRC	287.6714691591277	0.32625829575794885	2.166712
2	2024-01-11T11:49:41.496	SRC	287.6714691591277	0.32625829575794885	2.166712
2	2024-01-11T11:49:43.662	SRC	287.6713879825619	0.3261181469055727	2.166712
2	2024-01-11T11:49:43.662	SRC	287.6713879825619	0.3261181469055727	2.166712
2	2024-01-11T11:49:45.829	SRC	287.67090910633385	0.32652673443434777	2.166712
2	2024-01-11T11:49:45.829	SRC	287.67090910633385	0.32652673443434777	2.166712
2	2024-01-11T11:49:47.996	SRC	287.67124383627856	0.32706525258559205	2.166712
2	2024-01-11T11:49:47.996	SRC	287.67124383627856	0.32706525258559205	2.166712
2	2024-01-11T11:50:03.901	REFHOT	287.6742918175561	0.6655707220208467	2.166712
2	2024-01-11T11:50:03.901	REFHOT	287.6742918175561	0.6655707220208467	2.166712
2	2024-01-11T11:50:06.067	REFHOT	287.67416338171495	0.6659655152649732	2.166712
2	2024-01-11T11:50:06.067	REFHOT	287.67416338171495	0.6659655152649732	2.166712
2	2024-01-11T11:50:08.234	REFHOT	287.67399959769006	0.666113226504429	2.166712
2	2024-01-11T11:50:08.234	REFHOT	287.67399959769006	0.666113226504429	2.166712
2	2024-01-11T11:50:12.888	REF	287.67397015556793	0.6662910085989802	2.166712
2	2024-01-11T11:50:12.888	REF	287.67397015556793	0.6662910085989802	2.166712
2	2024-01-11T11:50:15.054	REF	287.67442930882487	0.6662625048811569	2.166712
2	2024-01-11T11:50:15.054	REF	287.67442930882487	0.6662625048811569	2.166712
2	2024-01-11T11:50:17.221	REF	287.6747353503409	0.6665545530915267	2.166712
2	2024-01-11T11:50:17.221	REF	287.6747353503409	0.6665545530915267	2.166712
2	2024-01-11T11:50:19.388	REF	287.67459802135863	0.6663639375978815	2.166712
2	2024-01-11T11:50:19.388	REF	287.67459802135863	0.6663639375978815	2.166712

Table 4: Table showing the timeline of the data in sequence 50 mixer 2. In this table, the mixer, the observation data and time per scan, the scan type, the galactic coordinates of the scan and the integration time are given. Note that every scan is duplicated.

Mixer	Observation Date and Time	Scan Type	Galactic Longitude	Galactic Latitude	Integration Time
3	2024-01-11T11:48:24.813	REFHOT	287.6502354013831	0.35432533070576766	2.166712
3	2024-01-11T11:48:24.813	REFHOT	287.6502354013831	0.35432533070576766	2.166712
3	2024-01-11T11:48:26.979	REFHOT	287.650234145366	0.3543251789553802	2.166712
3	2024-01-11T11:48:26.979	REFHOT	287.650234145366	0.3543251789553802	2.166712
3	2024-01-11T11:48:29.146	REFHOT	287.65023288850847	0.35432502729377324	2.166712
3	2024-01-11T11:48:29.146	REFHOT	287.65023288850847	0.35432502729377324	2.166712
3	2024-01-11T11:48:33.721	REF	287.65023023415785	0.35432470762553836	2.166712
3	2024-01-11T11:48:33.721	REF	287.65023023415785	0.35432470762553836	2.166712
3	2024-01-11T11:48:35.887	REF	287.65022897707	0.35432455652801365	2.166712
3	2024-01-11T11:48:35.887	REF	287.65022897707	0.35432455652801365	2.166712
3	2024-01-11T11:48:51.000	HOT	287.6491336683238	0.3538860544301678	2.166712
3	2024-01-11T11:48:51.000	HOT	287.6491336683238	0.3538860544301678	2.166712
3	2024-01-11T11:48:53.166	HOT	287.64980900957556	0.3540843020678465	2.166712
3	2024-01-11T11:48:53.166	HOT	287.64980900957556	0.3540843020678465	2.166712
3	2024-01-11T11:48:55.333	HOT	287.64991469424916	0.3541078715399185	2.166712
3	2024-01-11T11:48:55.333	HOT	287.64991469424916	0.3541078715399185	2.166712
3	2024-01-11T11:49:00.207	SRC	287.6494901720965	0.35398510216456175	2.166712
3	2024-01-11T11:49:00.207	SRC	287.6494901720965	0.35398510216456175	2.166712
3	2024-01-11T11:49:02.373	SRC	287.64959744461885	0.3542393640521657	2.166712
3	2024-01-11T11:49:02.373	SRC	287.64959744461885	0.3542393640521657	2.166712
3	2024-01-11T11:49:04.540	SRC	287.64926052060093	0.3538386765544893	2.166712
3	2024-01-11T11:49:04.540	SRC	287.64926052060093	0.3538386765544893	2.166712
3	2024-01-11T11:49:06.707	SRC	287.64943994041573	0.3536238763761959	2.166712
3	2024-01-11T11:49:06.707	SRC	287.64943994041573	0.3536238763761959	2.166712
3	2024-01-11T11:49:32.383	HOT	287.6506311747094	0.3536529828071146	2.166712
3	2024-01-11T11:49:32.383	HOT	287.6506311747094	0.3536529828071146	2.166712
3	2024-01-11T11:49:34.549	HOT	287.65038633593343	0.3533987407302978	2.166712
3	2024-01-11T11:49:34.549	HOT	287.65038633593343	0.3533987407302978	2.166712
3	2024-01-11T11:49:36.716	HOT	287.651429726546	0.35323236479908393	2.166712
3	2024-01-11T11:49:36.716	HOT	287.651429726546	0.35323236479908393	2.166712
3	2024-01-11T11:49:41.496	SRC	287.65074338920795	0.3533902850649211	2.166712
3	2024-01-11T11:49:41.496	SRC	287.65074338920795	0.3533902850649211	2.166712
3	2024-01-11T11:49:43.662	SRC	287.65066264555435	0.3532501185844214	2.166712
3	2024-01-11T11:49:43.662	SRC	287.65066264555435	0.3532501185844214	2.166712
3	2024-01-11T11:49:45.829	SRC	287.65018368534965	0.3536584508776572	2.166712
3	2024-01-11T11:49:45.829	SRC	287.65018368534965	0.3536584508776572	2.166712
3	2024-01-11T11:49:47.996	SRC	287.65051903965286	0.3541972464130566	2.166712
3	2024-01-11T11:49:47.996	SRC	287.65051903965286	0.3541972464130566	2.166712
3	2024-01-11T11:50:03.901	REFHOT	287.653478095498	0.6927174537704522	2.166712
3	2024-01-11T11:50:03.901	REFHOT	287.653478095498	0.6927174537704522	2.166712
3	2024-01-11T11:50:06.067	REFHOT	287.6533498997807	0.6931122183533743	2.166712
3	2024-01-11T11:50:06.067	REFHOT	287.6533498997807	0.6931122183533743	2.166712
3	2024-01-11T11:50:08.234	REFHOT	287.65318639387965	0.6932598690420199	2.166712
3	2024-01-11T11:50:08.234	REFHOT	287.65318639387965	0.6932598690420199	2.166712
3	2024-01-11T11:50:12.888	REF	287.6531578803251	0.6934377235285961	2.166712
3	2024-01-11T11:50:12.888	REF	287.6531578803251	0.6934377235285961	2.166712
3	2024-01-11T11:50:15.054	REF	287.6536179259903	0.6934095543947218	2.166712
3	2024-01-11T11:50:15.054	REF	287.6536179259903	0.6934095543947218	2.166712
3	2024-01-11T11:50:17.221	REF	287.65392463017713	0.6937018498778402	2.166712
3	2024-01-11T11:50:17.221	REF	287.65392463017713	0.6937018498778402	2.166712
3	2024-01-11T11:50:19.388	REF	287.65378769822684	0.6935111778998961	2.166712
3	2024-01-11T11:50:19.388	REF	287.65378769822684	0.6935111778998961	2.166712

Table 5: Table showing the timeline of the data in sequence 50 mixer 3. In this table, the mixer, the observation data and time per scan, the scan type, the galactic coordinates of the scan and the integration time are given. Note that every scan is duplicated.

Mixer	Observation Date and Time	Scan Type	Galactic Longitude	Galactic Latitude	Integration Time
2	2024-01-11T11:50:26.055	REFHOT	287.67209605452155	0.32642731589576457	2.166712
2	2024-01-11T11:50:26.055	REFHOT	287.67209605452155	0.32642731589576457	2.166712
2	2024-01-11T11:50:28.221	REFHOT	287.67209432048156	0.3264271337924727	2.166712
2	2024-01-11T11:50:28.221	REFHOT	287.67209432048156	0.3264271337924727	2.166712
2	2024-01-11T11:50:30.388	REFHOT	287.6720925855786	0.32642695191053195	2.166712
2	2024-01-11T11:50:30.388	REFHOT	287.6720925855786	0.32642695191053195	2.166712
2	2024-01-11T11:50:34.959	REF	287.6720889258257	0.32642656925656527	2.166712
2	2024-01-11T11:50:34.959	REF	287.6720889258257	0.32642656925656527	2.166712
2	2024-01-11T11:50:51.841	HOT	287.67201165058907	0.32628551688669866	2.166712
2	2024-01-11T11:50:51.841	HOT	287.67201165058907	0.32628551688669866	2.166712
2	2024-01-11T11:50:54.007	HOT	287.67202461324104	0.32614724193071615	2.166712
2	2024-01-11T11:50:54.007	HOT	287.67202461324104	0.32614724193071615	2.166712
2	2024-01-11T11:50:56.174	HOT	287.67214729590194	0.326432454469669	2.166712
2	2024-01-11T11:50:56.174	HOT	287.67214729590194	0.326432454469669	2.166712
2	2024-01-11T11:51:00.920	SRC	287.67185885131147	0.3265555876924703	2.166712
2	2024-01-11T11:51:00.920	SRC	287.67185885131147	0.3265555876924703	2.166712
2	2024-01-11T11:51:03.086	SRC	287.6718178887983	0.326772978744709	2.166712
2	2024-01-11T11:51:03.086	SRC	287.6718178887983	0.326772978744709	2.166712
2	2024-01-11T11:51:05.253	SRC	287.67196709430544	0.3268188467408767	2.166712
2	2024-01-11T11:51:05.253	SRC	287.67196709430544	0.3268188467408767	2.166712
2	2024-01-11T11:51:07.420	SRC	287.6724305536952	0.32649575262010927	2.166712
2	2024-01-11T11:51:07.420	SRC	287.6724305536952	0.32649575262010927	2.166712
2	2024-01-11T11:53:16.207	HOT	287.67087487659444	0.32697366508085324	3.0000637
2	2024-01-11T11:53:16.207	HOT	287.67087487659444	0.32697366508085324	3.0000637
2	2024-01-11T11:53:19.207	HOT	287.6707585445042	0.32683894754401305	3.0000637
2	2024-01-11T11:53:19.207	HOT	287.6707585445042	0.32683894754401305	3.0000637
2	2024-01-11T11:53:22.207	HOT	287.67044210801294	0.3263650498714749	3.0000637
2	2024-01-11T11:53:22.207	HOT	287.67044210801294	0.3263650498714749	3.0000637
2	2024-01-11T11:53:27.703	SRC	287.67004817014856	0.32674132759719465	3.0000637
2	2024-01-11T11:53:27.703	SRC	287.67004817014856	0.32674132759719465	3.0000637
2	2024-01-11T11:53:30.703	SRC	287.67030233538844	0.32707834062088853	3.0000637
2	2024-01-11T11:53:30.703	SRC	287.67030233538844	0.32707834062088853	3.0000637
2	2024-01-11T11:53:43.838	HOT	287.79922933263447	0.3569134927123178	3.0000637
2	2024-01-11T11:53:43.838	HOT	287.79922933263447	0.3569134927123178	3.0000637
2	2024-01-11T11:53:46.838	HOT	287.7994479075518	0.3567568840802515	3.0000637
2	2024-01-11T11:53:46.838	HOT	287.7994479075518	0.3567568840802515	3.0000637
2	2024-01-11T11:53:49.838	HOT	287.79914465781746	0.3570716777366197	3.0000637
2	2024-01-11T11:53:49.838	HOT	287.79914465781746	0.3570716777366197	3.0000637
2	2024-01-11T11:53:55.230	SRC	287.79885807330675	0.3570668378397518	3.0000637
2	2024-01-11T11:53:55.230	SRC	287.79885807330675	0.3570668378397518	3.0000637
2	2024-01-11T11:53:58.230	SRC	287.799311214016	0.3568524420781824	3.0000637
2	2024-01-11T11:53:58.230	SRC	287.799311214016	0.3568524420781824	3.0000637
2	2024-01-11T11:54:09.353	HOT	287.8292878113983	0.22696832182756352	3.0000637
2	2024-01-11T11:54:09.353	HOT	287.8292878113983	0.22696832182756352	3.0000637
2	2024-01-11T11:54:12.353	HOT	287.8294367223813	0.22751114177516543	3.0000637
2	2024-01-11T11:54:12.353	HOT	287.8294367223813	0.22751114177516543	3.0000637
2	2024-01-11T11:54:15.353	HOT	287.82879897944935	0.2270373405780339	3.0000637
2	2024-01-11T11:54:15.353	HOT	287.82879897944935	0.2270373405780339	3.0000637
2	2024-01-11T11:54:20.737	SRC	287.8296782453082	0.22728390075678193	3.0000637
2	2024-01-11T11:54:20.737	SRC	287.8296782453082	0.22728390075678193	3.0000637
2	2024-01-11T11:54:23.737	SRC	287.8286507942158	0.22694242843061715	3.0000637
2	2024-01-11T11:54:23.737	SRC	287.8286507942158	0.22694242843061715	3.0000637
2	2024-01-11T11:54:35.393	HOT	287.7000990287596	0.19648874646064768	3.0000637
2	2024-01-11T11:54:35.393	HOT	287.7000990287596	0.19648874646064768	3.0000637
2	2024-01-11T11:54:38.393	HOT	287.70017353582347	0.19688031017455204	3.0000637
2	2024-01-11T11:54:38.393	HOT	287.70017353582347	0.19688031017455204	3.0000637
2	2024-01-11T11:54:41.393	HOT	287.7001384696769	0.1972543926167652	3.0000637
2	2024-01-11T11:54:41.393	HOT	287.7001384696769	0.1972543926167652	3.0000637
2	2024-01-11T11:54:47.003	SRC	287.6999721067398	0.19676533821091277	3.0000637
2	2024-01-11T11:54:47.003	SRC	287.6999721067398	0.19676533821091277	3.0000637
2	2024-01-11T11:54:50.003	SRC	287.70002109427435	0.19705192689455991	3.0000637

Table 6: Table showing part 1 of the timeline of the data in sequence 51 mixer 2. In this table, the mixer, the observation data and time per scan, the scan type, the galactic coordinates of the scan and the integration time are given. Note that every scan is duplicated.

Mixer	Observation Date and Time	Scan Type	Galactic Longitude	Galactic Latitude	Integration Time
2	2024-01-11T11:54:50.003	SRC	287.70002109427435	0.19705192689455991	3.0000637
2	2024-01-11T11:55:03.167	HOT	287.57100338448095	0.16677336844086194	3.0000637
2	2024-01-11T11:55:03.167	HOT	287.57100338448095	0.16677336844086194	3.0000637
2	2024-01-11T11:55:06.167	HOT	287.57129859907207	0.1669338389941278	3.0000637
2	2024-01-11T11:55:06.167	HOT	287.57129859907207	0.1669338389941278	3.0000637
2	2024-01-11T11:55:09.167	HOT	287.5704729112405	0.167009645277321	3.0000637
2	2024-01-11T11:55:09.167	HOT	287.5704729112405	0.167009645277321	3.0000637
2	2024-01-11T11:55:14.873	SRC	287.57060887381186	0.16676665828772452	3.0000637
2	2024-01-11T11:55:14.873	SRC	287.57060887381186	0.16676665828772452	3.0000637
2	2024-01-11T11:55:17.873	SRC	287.5708759230936	0.16693569666463828	3.0000637
2	2024-01-11T11:55:17.873	SRC	287.5708759230936	0.16693569666463828	3.0000637
2	2024-01-11T11:55:28.405	HOT	287.5413227325197	0.2968463587707814	3.0000637
2	2024-01-11T11:55:28.405	HOT	287.5413227325197	0.2968463587707814	3.0000637
2	2024-01-11T11:55:31.405	HOT	287.5414841024123	0.29615488834091147	3.0000637
2	2024-01-11T11:55:31.405	HOT	287.5414841024123	0.29615488834091147	3.0000637
2	2024-01-11T11:55:34.405	HOT	287.541433695029	0.2967441631403557	3.0000637
2	2024-01-11T11:55:34.405	HOT	287.541433695029	0.2967441631403557	3.0000637
2	2024-01-11T11:55:39.908	SRC	287.5421352921039	0.2966222845250991	3.0000637
2	2024-01-11T11:55:39.908	SRC	287.5421352921039	0.2966222845250991	3.0000637
2	2024-01-11T11:55:42.908	SRC	287.54232328896836	0.2963282680093243	3.0000637
2	2024-01-11T11:55:42.908	SRC	287.54232328896836	0.2963282680093243	3.0000637
2	2024-01-11T11:55:53.615	HOT	287.51244083604576	0.42677137334015675	3.0000637
2	2024-01-11T11:55:53.615	HOT	287.51244083604576	0.42677137334015675	3.0000637
2	2024-01-11T11:55:56.615	HOT	287.51239846603045	0.42692720634751885	3.0000637
2	2024-01-11T11:55:56.615	HOT	287.51239846603045	0.42692720634751885	3.0000637
2	2024-01-11T11:55:59.615	HOT	287.51279356883055	0.4265396299073418	3.0000637
2	2024-01-11T11:55:59.615	HOT	287.51279356883055	0.4265396299073418	3.0000637
2	2024-01-11T11:56:05.018	SRC	287.5127134959762	0.4265159029672727	3.0000637
2	2024-01-11T11:56:05.018	SRC	287.5127134959762	0.4265159029672727	3.0000637
2	2024-01-11T11:56:08.018	SRC	287.5125315308126	0.42650825734854886	3.0000637
2	2024-01-11T11:56:08.018	SRC	287.5125315308126	0.42650825734854886	3.0000637
2	2024-01-11T11:56:20.361	HOT	287.64148280534977	0.4566467509800881	3.0000637
2	2024-01-11T11:56:20.361	HOT	287.64148280534977	0.4566467509800881	3.0000637
2	2024-01-11T11:56:23.361	HOT	287.6419281095186	0.45640640344811806	3.0000637
2	2024-01-11T11:56:23.361	HOT	287.6419281095186	0.45640640344811806	3.0000637
2	2024-01-11T11:56:26.361	HOT	287.64209026967103	0.4561756808680711	3.0000637
2	2024-01-11T11:56:26.361	HOT	287.64209026967103	0.4561756808680711	3.0000637
2	2024-01-11T11:56:32.042	SRC	287.6412679042834	0.45622024438762154	3.0000637
2	2024-01-11T11:56:32.042	SRC	287.6412679042834	0.45622024438762154	3.0000637
2	2024-01-11T11:56:35.042	SRC	287.642558373683	0.45616327570403287	3.0000637
2	2024-01-11T11:56:35.042	SRC	287.642558373683	0.45616327570403287	3.0000637
2	2024-01-11T11:56:47.016	HOT	287.7707562243304	0.4864550486527105	3.0000637
2	2024-01-11T11:56:47.016	HOT	287.7707562243304	0.4864550486527105	3.0000637
2	2024-01-11T11:56:50.016	HOT	287.771221787976	0.48640710086659467	3.0000637
2	2024-01-11T11:56:50.016	HOT	287.771221787976	0.48640710086659467	3.0000637
2	2024-01-11T11:56:53.016	HOT	287.771115879284	0.48618679052295366	3.0000637
2	2024-01-11T11:56:53.016	HOT	287.771115879284	0.48618679052295366	3.0000637
2	2024-01-11T11:56:58.617	SRC	287.7714208013478	0.4862807136379641	3.0000637
2	2024-01-11T11:56:58.617	SRC	287.7714208013478	0.4862807136379641	3.0000637
2	2024-01-11T11:57:01.617	SRC	287.7714761043663	0.4858815001115684	3.0000637
2	2024-01-11T11:57:01.617	SRC	287.7714761043663	0.4858815001115684	3.0000637

Table 7: Table showing part 2 of the timeline of the data in sequence 51 mixer 2. In this table, the mixer, the observation data and time per scan, the scan type, the galactic coordinates of the scan and the integration time are given. Note that every scan is duplicated.

Mixer	Observation Date and Time	Scan Type	Galactic Longitude	Galactic Latitude	Integration Time
3	2024-01-11T11:50:26.055	REFHOT	287.6513828499209	0.3535652712374782	2.166712
3	2024-01-11T11:50:26.055	REFHOT	287.6513828499209	0.3535652712374782	2.166712
3	2024-01-11T11:50:28.221	REFHOT	287.65138158104907	0.3535651268131828	2.166712
3	2024-01-11T11:50:28.221	REFHOT	287.65138158104907	0.3535651268131828	2.166712
3	2024-01-11T11:50:30.388	REFHOT	287.65138031133097	0.35356498248105533	2.166712
3	2024-01-11T11:50:30.388	REFHOT	287.65138031133097	0.35356498248105533	2.166712
3	2024-01-11T11:50:34.959	REF	287.65137763217405	0.35356467855263335	2.166712
3	2024-01-11T11:50:34.959	REF	287.65137763217405	0.35356467855263335	2.166712
3	2024-01-11T11:50:37.125	REF	287.65137636223227	0.3535645347809793	2.166712
3	2024-01-11T11:50:37.125	REF	287.65137636223227	0.3535645347809793	2.166712
3	2024-01-11T11:50:51.841	HOT	287.6513039513978	0.35342386467740755	2.166712
3	2024-01-11T11:50:51.841	HOT	287.6513039513978	0.35342386467740755	2.166712
3	2024-01-11T11:50:54.007	HOT	287.6513174288061	0.35328563002125524	2.166712
3	2024-01-11T11:50:54.007	HOT	287.6513174288061	0.35328563002125524	2.166712
3	2024-01-11T11:50:56.174	HOT	287.6514406087954	0.3535709698036252	2.166712
3	2024-01-11T11:50:56.174	HOT	287.6514406087954	0.3535709698036252	2.166712
3	2024-01-11T11:51:00.920	SRC	287.6511528818375	0.3536940008095282	2.166712
3	2024-01-11T11:51:00.920	SRC	287.6511528818375	0.3536940008095282	2.166712
3	2024-01-11T11:51:03.086	SRC	287.6511122847156	0.3539114098687313	2.166712
3	2024-01-11T11:51:03.086	SRC	287.6511122847156	0.3539114098687313	2.166712
3	2024-01-11T11:51:05.253	SRC	287.65126207774415	0.3539574127534828	2.166712
3	2024-01-11T11:51:05.253	SRC	287.65126207774415	0.3539574127534828	2.166712
3	2024-01-11T11:51:07.420	SRC	287.65172651536375	0.3536346435410844	2.166712
3	2024-01-11T11:51:07.420	SRC	287.65172651536375	0.3536346435410844	2.166712
3	2024-01-11T11:53:16.207	HOT	287.6501964548387	0.35411344926582383	3.0000637
3	2024-01-11T11:53:16.207	HOT	287.6501964548387	0.35411344926582383	3.0000637
3	2024-01-11T11:53:19.207	HOT	287.6500806778805	0.35397868872847343	3.0000637
3	2024-01-11T11:53:19.207	HOT	287.6500806778805	0.35397868872847343	3.0000637
3	2024-01-11T11:53:22.207	HOT	287.64976470644575	0.3535046048458309	3.0000637
3	2024-01-11T11:53:22.207	HOT	287.64976470644575	0.3535046048458309	3.0000637
3	2024-01-11T11:53:27.703	SRC	287.64937144420935	0.3538807083950329	3.0000637
3	2024-01-11T11:53:27.703	SRC	287.64937144420935	0.3538807083950329	3.0000637
3	2024-01-11T11:53:30.703	SRC	287.6496263725849	0.3542179360609438	3.0000637
3	2024-01-11T11:53:30.703	SRC	287.6496263725849	0.3542179360609438	3.0000637
3	2024-01-11T11:53:43.838	HOT	287.7786664561407	0.38413799022483525	3.0000637
3	2024-01-11T11:53:43.838	HOT	287.7786664561407	0.38413799022483525	3.0000637
3	2024-01-11T11:53:46.838	HOT	287.7788859061164	0.3839815559534219	3.0000637
3	2024-01-11T11:53:46.838	HOT	287.7788859061164	0.3839815559534219	3.0000637
3	2024-01-11T11:53:49.838	HOT	287.77858291723385	0.3842962031277106	3.0000637
3	2024-01-11T11:53:49.838	HOT	287.77858291723385	0.3842962031277106	3.0000637
3	2024-01-11T11:53:55.230	SRC	287.77829719959084	0.3842912457888471	3.0000637
3	2024-01-11T11:53:55.230	SRC	287.77829719959084	0.3842912457888471	3.0000637
3	2024-01-11T11:53:58.230	SRC	287.7787514464497	0.38407717303321737	3.0000637
3	2024-01-11T11:53:58.230	SRC	287.7787514464497	0.38407717303321737	3.0000637
3	2024-01-11T11:54:09.353	HOT	287.8087945985104	0.25420788304839204	3.0000637
3	2024-01-11T11:54:09.353	HOT	287.8087945985104	0.25420788304839204	3.0000637
3	2024-01-11T11:54:12.353	HOT	287.8089441217988	0.2547508556283684	3.0000637
3	2024-01-11T11:54:12.353	HOT	287.8089441217988	0.2547508556283684	3.0000637
3	2024-01-11T11:54:15.353	HOT	287.808306547489	0.2542766600740448	3.0000637
3	2024-01-11T11:54:15.353	HOT	287.808306547489	0.2542766600740448	3.0000637
3	2024-01-11T11:54:20.737	SRC	287.809187681751	0.25452386306608815	3.0000637
3	2024-01-11T11:54:20.737	SRC	287.809187681751	0.25452386306608815	3.0000637
3	2024-01-11T11:54:23.737	SRC	287.80815999990045	0.2541817478314415	3.0000637
3	2024-01-11T11:54:23.737	SRC	287.80815999990045	0.2541817478314415	3.0000637
3	2024-01-11T11:54:35.393	HOT	287.67950012187083	0.2236435198986049	3.0000637
3	2024-01-11T11:54:35.393	HOT	287.67950012187083	0.2236435198986049	3.0000637

Table 8: Table showing part 1 of the timeline of the data in sequence 51 mixer 3. In this table, the mixer, the observation data and time per scan, the scan type, the galactic coordinates of the scan and the integration time are given. Note that every scan is duplicated.

Mixer	Observation Date and Time	Scan Type	Galactic Longitude	Galactic Latitude	Integration Time
3	2024-01-11T11:54:38.393	HOT	287.6795752043671	0.22403517744014437	3.0000637
3	2024-01-11T11:54:38.393	HOT	287.6795752043671	0.22403517744014437	3.0000637
3	2024-01-11T11:54:41.393	HOT	287.679540616741	0.22440928135774899	3.0000637
3	2024-01-11T11:54:41.393	HOT	287.679540616741	0.22440928135774899	3.0000637
3	2024-01-11T11:54:47.003	SRC	287.6793753831807	0.22392015548519065	3.0000637
3	2024-01-11T11:54:47.003	SRC	287.6793753831807	0.22392015548519065	3.0000637
3	2024-01-11T11:54:50.003	SRC	287.67942495009703	0.22420681628988762	3.0000637
3	2024-01-11T11:54:50.003	SRC	287.67942495009703	0.22420681628988762	3.0000637
3	2024-01-11T11:55:03.167	HOT	287.5502989288334	0.19384286902984496	3.0000637
3	2024-01-11T11:55:03.167	HOT	287.5502989288334	0.19384286902984496	3.0000637
3	2024-01-11T11:55:06.167	HOT	287.5505949751907	0.19400356357836257	3.0000637
3	2024-01-11T11:55:06.167	HOT	287.5505949751907	0.19400356357836257	3.0000637
3	2024-01-11T11:55:09.167	HOT	287.5497691060797	0.1940788554622096	3.0000637
3	2024-01-11T11:55:09.167	HOT	287.5497691060797	0.1940788554622096	3.0000637
3	2024-01-11T11:55:14.873	SRC	287.5499064051098	0.19383599250875574	3.0000637
3	2024-01-11T11:55:14.873	SRC	287.5499064051098	0.19383599250875574	3.0000637
3	2024-01-11T11:55:17.873	SRC	287.5501742563204	0.194005235669982	3.0000637
3	2024-01-11T11:55:17.873	SRC	287.5501742563204	0.194005235669982	3.0000637
3	2024-01-11T11:55:28.405	HOT	287.5205604167525	0.32390175065356575	3.0000637
3	2024-01-11T11:55:28.405	HOT	287.5205604167525	0.32390175065356575	3.0000637
3	2024-01-11T11:55:31.405	HOT	287.5207227236555	0.32321038023155707	3.0000637
3	2024-01-11T11:55:31.405	HOT	287.5207227236555	0.32321038023155707	3.0000637
3	2024-01-11T11:55:34.405	HOT	287.5206727072693	0.3237996666213531	3.0000637
3	2024-01-11T11:55:34.405	HOT	287.5206727072693	0.3237996666213531	3.0000637
3	2024-01-11T11:55:39.908	SRC	287.5213760809844	0.3236782811624985	3.0000637
3	2024-01-11T11:55:39.908	SRC	287.5213760809844	0.3236782811624985	3.0000637
3	2024-01-11T11:55:42.908	SRC	287.52156492914077	0.3233843967292726	3.0000637
3	2024-01-11T11:55:42.908	SRC	287.52156492914077	0.3233843967292726	3.0000637
3	2024-01-11T11:55:53.615	HOT	287.4916213572753	0.45381314956657604	3.0000637
3	2024-01-11T11:55:53.615	HOT	287.4916213572753	0.45381314956657604	3.0000637
3	2024-01-11T11:55:56.615	HOT	287.4915795011442	0.453968980115231	3.0000637
3	2024-01-11T11:55:56.615	HOT	287.4915795011442	0.453968980115231	3.0000637
3	2024-01-11T11:55:59.615	HOT	287.4919756680744	0.45358166585836357	3.0000637
3	2024-01-11T11:55:59.615	HOT	287.4919756680744	0.45358166585836357	3.0000637
3	2024-01-11T11:56:05.018	SRC	287.4918965992959	0.4535579188292709	3.0000637
3	2024-01-11T11:56:05.018	SRC	287.4918965992959	0.4535579188292709	3.0000637
3	2024-01-11T11:56:08.018	SRC	287.49171506342833	0.45355017186896046	3.0000637
3	2024-01-11T11:56:08.018	SRC	287.49171506342833	0.45355017186896046	3.0000637
3	2024-01-11T11:56:20.361	HOT	287.62077887506587	0.48377409369315205	3.0000637
3	2024-01-11T11:56:20.361	HOT	287.62077887506587	0.48377409369315205	3.0000637
3	2024-01-11T11:56:23.361	HOT	287.62122525607674	0.48353404729638944	3.0000637
3	2024-01-11T11:56:23.361	HOT	287.62122525607674	0.48353404729638944	3.0000637
3	2024-01-11T11:56:26.361	HOT	287.62138822972247	0.483303441566496	3.0000637
3	2024-01-11T11:56:26.361	HOT	287.62138822972247	0.483303441566496	3.0000637
3	2024-01-11T11:56:32.042	SRC	287.620566231069	0.4833475082546865	3.0000637
3	2024-01-11T11:56:32.042	SRC	287.620566231069	0.4833475082546865	3.0000637
3	2024-01-11T11:56:35.042	SRC	287.6218585020302	0.48329139702508944	3.0000637
3	2024-01-11T11:56:35.042	SRC	287.6218585020302	0.48329139702508944	3.0000637
3	2024-01-11T11:56:47.016	HOT	287.75016827564116	0.5136676493334141	3.0000637
3	2024-01-11T11:56:47.016	HOT	287.75016827564116	0.5136676493334141	3.0000637
3	2024-01-11T11:56:50.016	HOT	287.75063488728756	0.5136200227858323	3.0000637
3	2024-01-11T11:56:50.016	HOT	287.75063488728756	0.5136200227858323	3.0000637
3	2024-01-11T11:56:53.016	HOT	287.75052954824287	0.5133996568832909	3.0000637
3	2024-01-11T11:56:53.016	HOT	287.75052954824287	0.5133996568832909	3.0000637
3	2024-01-11T11:56:58.617	SRC	287.75083585343054	0.5134938195719441	3.0000637
3	2024-01-11T11:56:58.617	SRC	287.75083585343054	0.5134938195719441	3.0000637
3	2024-01-11T11:57:01.617	SRC	287.75089192408217	0.513094647635579	3.0000637
3	2024-01-11T11:57:01.617	SRC	287.75089192408217	0.513094647635579	3.0000637

Table 9: Table showing part 2 of the timeline of the data in sequence 51 mixer 3. In this table, the mixer, the observation data and time per scan, the scan type, the galactic coordinates of the scan and the integration time are given. Note that every scan is duplicated.